



Contents lists available at ScienceDirect

Transportation Research Part B

journal homepage: www.elsevier.com/locate/trb



Analytical approximation and calibration of roundabout capacity: A merging state transition-based modeling approach

Yang Song ^a, Xianbiao Hu ^{b,*}, Jiawei Lu ^c, Xuesong Zhou ^c

^a Department of Civil and Environmental Engineering, Pennsylvania State University, University Park, PA 16802-1408, USA

^b Department of Civil and Environmental Engineering, Pennsylvania State University, 212 Sackett Building, University Park, PA 16802-1408, USA

^c School of Sustainable Engineering and the Built Environment, Arizona State University, College Avenue Commons, Room 474, 660 S. College Avenue, Tempe, AZ 85287, USA



ARTICLE INFO

Keywords:

Roundabout capacity
State transition
State-space-time diagram
Vehicle kinematics
Critical gap

ABSTRACT

This manuscript focuses on the theoretical advancement of causality between entry vehicle dynamics and roundabout capacity modeling, with a merging state transition-based analytical approximation and calibration approach. Gap acceptance models, such as the HCM model, usually ignore roundabout specific operating conditions, whereas empirical models are generally criticized for the lack of fundamental understanding of underlying traffic flow or driving behaviors. The roundabout geometry is firstly extracted into a Y-shaped network, and the traffic movements are illustrated with a state-space-time diagram. Next, we analyze the merging state space for the entry vehicles, and draw the state-transition diagram. The episode of a traffic flow is defined, and we show that the trajectory of an entry vehicle repeats one of four patterns within each episode. Then, state transition-based analytical derivation of roundabout capacity is presented. This is done by estimating the state transition probabilities, followed by an episode-based state transition chain analysis and, finally, finding the solution of state transitions under steady states. Circulating speed is used as a key variable to reflect the operating conditions in the target roundabout. For a special scenario, with all four entry approaches being saturated, we model the interactions between entry flow and circulating flow, and prove that the resulting model can be uniquely solved by classic root-finding algorithms. The accuracy of the proposed model is tested with OpenDD, a real-world high-resolution trajectory dataset collected by drones at four roundabouts. The results of the proposed model are shown to consistently outperform the HCM6 model and another gap acceptance-based model.

1. Introduction

A roundabout, which is defined as an unsignalized circular intersection where traffic moves in a one-way direction around a central island (Chen and Hourdos 2018), has been shown conclusively to enhance safety at an intersection by reducing the number of conflict points, as well as travel speed if well designed (Kácovský et al., 2019). Central to an effective roundabout design and the determination of its adoption at a particular intersection, is an accurate prediction of roundabout capacity. Per Yap et al. (2013), the definition of roundabout capacity is the maximum inflow from a roundabout entry, with saturated demand, where at least one vehicle is always queued at the give-way line of the entry lane, ready to enter any available acceptable gap in the circulating stream.

* Corresponding author.

E-mail address: xbhu@psu.edu (X. Hu).

Gap acceptance is a common approach to modelling roundabout entry flow capacity Q_e , with conflicting traffic flow (or circulating traffic flow) Q_c , critical gap t_c , follow-up headway t_f , and distribution of gaps in circulating flow (usually follows negative exponential distribution), as the four main input data. Examples of gap acceptance-based models include Akcelik (1994), Rodegerdts et al. (2007), Brilon et al. (1997), Troutbeck (1989), Wu (2001) and many others. A critical gap is required in the gap acceptance model to predict roundabout capacity, and a common strategy is to adopt a fixed value, such as those suggested by Highway Capacity Manual (HCM) or other references. Such a fixed value of a critical gap, however, when adopted, ignores the operating conditions, as well as the geometric factors of a roundabout. This shortcoming of a gap-acceptance model has been criticized by many in the literature, as summarized by Yap et al. (2013). Calibration of a critical gap at each location, on the other hand, is labor-intensive and unrealistic. An empirical modeling approach is another commonly seen method for determining roundabout capacity, with the key idea of developing regression models to reflect the relationships between geometry and actual measured capacity. Most empirical models are developed based on linear or exponential regression forms, with $Q_e = A - BQ_c$ or $Q_e = A^* \exp(BQ_c)$, in which A and B represent the intercept and slope constants, respectively. Such a modeling approach, however, is generally criticized for poor transferability, as well as a lack of fundamental understanding of underlying traffic flow or driving behaviors.

To overcome these issues, this manuscript aims to advance the causality and theoretical understanding of roundabout capacity modeling, with a merging state transition-based analytical approximation and calibration approach. Our work is inspired by Larson and Odoni (1981), who proposed a state-based analytical approach to analyze the relationships between demand on a service system and the delays suffered by the users of that system. In our context, the studied service system refers to the roundabout traffic dynamics, with conflicts between entry vehicles (which represent demand) and circulating vehicles (which determines the discharge rate, or service capacity). First, we examine the kinematics of the vehicles entering a roundabout with a state-space-time representation approach. The roundabout geometry is extracted into a Y-shaped network, with an additional dummy node to represent the entry vehicle's waiting behavior. Next, we analyze the merging state space for the roundabout entry vehicles $S = \{S_1, S_2, S_3\}$, including a state that a merging vehicle has to stop and wait for an acceptable gap (i.e., wait state S_1), or accelerates and then merges (i.e., acceleration state S_2), or merges without experiencing a full-stop (i.e., following state S_3). We then draw the state-transition diagram by enumerating all possible state transition combinations between them, and demonstrate the Markov chain property, i.e., the state of a merging vehicle is only affected by its immediate leading state, but not the others. The episode of a traffic flow is then defined, and we show that the trajectory of an entry vehicle repeats patterns within each episode, i.e., an episode always starts with an entry vehicle that experiences a full stop, followed by a platoon of succeeding vehicles and, finally, ends with another entry vehicle that experiences a full stop.

The traffic arrivals are assumed to follow Poisson distribution. Learning from vehicle kinematics and crash avoidance requirements, the headway thresholds for a vehicle to merge into a roundabout can be formulated as a function of circulating speed, as well as the driver's needed perception-response time, and the vehicle's maximum deceleration. In particular, we note that the usage of circulating speed in the proposed model will not only serve a similar purpose as a critical gap in a gap-acceptance model, but it is also able to reflect the operating conditions and circle radius that are specifically related with the roundabout of interest. Calibration of circulating speed is also relatively easy with existing data sources; for example, with the partial vehicle trajectory data from a smartphone, connected vehicles, or collected by drones as demonstrated in the case study of this manuscript.

Built upon these theoretical analysis and properties, the state transition-based analytical derivation of roundabout capacity is then presented. This is done by firstly estimating the state transition probabilities between any two nodes in the state transition diagram. Then, we enumerate all possible state transition chains, or Markov chain categories, within one episode, and calculate their probabilities. Finally, we derive the roundabout capacity by finding the solution of state transitions under steady states, which is computed based on the relationship between the state transition chains and the number of vehicles that can merge into the roundabout in each chain. In addition, we also model a special scenario where all four entry approaches are saturated, and thus the interactions between entry flow and circulating flow exist, and allow us to add an additional constraint to the original problem to solve the equation set. We analytically prove that the resulted model for this special scenario generates a monotonously decreasing function, and, thus, a unique solution can be obtained by classic root-finding algorithms such as Newton's method.

The remainder of this manuscript is organized as follows. Section 2 summarizes relevant literature. Section 3 performs analytical analysis on the roundabout traffic dynamics, and discusses the theoretical properties with a state-based analytical approach. The analytical derivation of roundabout capacity is presented in Section 4. Section 5 provides a numerical analysis with openDD, a real-world high-resolution trajectory dataset, and HCM6 model is used as a benchmark for comparison purposes. Finally, concluding remarks are given in Section 6.

2. Literature review

The empirical modeling approach, in which regression models are built based on relationships between geometry and actual measured capacity, is the longest established form of roundabout capacity estimation. Most empirical models are developed based on linear or exponential regression forms, with $Q_e = A - BQ_c$ or $Q_e = A^* \exp(BQ_c)$, in which A and B represent the intercept and slope constants, respectively. Expression for the constants may also be developed, e.g., as a function of other parameters such as roundabout geometry (Rodegerdts 2007; Rodegerdts et al., 2007). For example, Federal Highway Administration uses $Q_e = 1218 - 0.74Q_c$ for urban compact roundabout, $Q_e = \min(1212 - 0.5447Q_c, 1800 - Q_c)$ for a single-lane roundabout, and $Q_e = 2424 - 0.7159Q_c$ for a double-lane roundabout (Robinson et al., 2010). Other examples of empirical models include (Yap et al., 2015), in which two regression models and an artificial neural network are developed, with data from 35 roundabout entry lanes in U.K. Brilon and Stuwe (1993) find that geometric parameters, including inscribed circle diameter, number of traffic circle arms, and distance between exit

and entry of the observed arm play significant role in roundabout capacity in Germany. Pilko et al. (2017) formulate roundabout capacity as a function of several geometry parameters, such as entry angle, entry radius, flare length elements, and inscribed circle diameter, and further propose a multi-criterion approach to optimize the capacity. In addition, based on field data collected at nine roundabouts in Australia, Ren et al. (2016) evaluate the performance of the capacity estimation for single-lane roundabouts with 5 models.

Other than linear or exponential regression models, advanced machine learning models have also been developed for roundabout capacity estimation. For example, neural networks are adopted to explore the complex and non-linear relationship between input variables and entering capacities (Karlaftis and Vlahogianni 2011), since the performances of statistical regression models are constrained by a priori knowledge in the form of relationships between independent and dependent variables. Özysal et al. (2009) develop an artificial neural network model to predict entry capacity with geometric parameters, as the most reliable estimator, which is shown to outperform gap acceptance and regression models. Patnaik et al. (2020) develop Genetic Algorithm, multi-variate adaptive regression spline and random forest regression models to estimate roundabout capacity. Research on additional empirical models can also be found in (Kimber 1980; Simon 1991; Stuwe 1991; Polus and Shmueli 1997; Valdez et al., 2011; Pompigna et al., 2020), among others.

Empirical models are generally criticized for their poor transferability, as well as a lack of fundamental understanding of underlying traffic flow or driving behaviors. Gap acceptance, on the other hand, is another modeling approach that aims to amend these issues. Those models are mainly built on measurements of headways, from both circulating flow and entering flow, with the core idea of exploring how a driver's behavior, in terms of gap acceptance of time headways, impacted the entry capacity of a roundabout. Gap acceptance models usually require four types of input data, including (1) critical gap, which is the minimum time headway in the circulating flow stream that an entering vehicle could accept and is not a constant and typically follows a log-normal distribution; (2) the conflicting traffic flow (or circulating traffic flow) Q_c ; (3) follow-up headway, which is the time headway between two consecutive queued vehicles entering the same gap in the circulating flow stream and, finally, (4) distribution of gaps in a circulating flow, which is usually based on Poissonian random arrivals or bunched flows (Rodegerdts et al., 2007; Yap et al., 2013). In this way, compared with empirical models, the data collection demand of analytical methods is less contingent, especially with heavily-congested entries in continuous queuing (Akcelik et al., 1998).

In the 2010 version of the Highway Capacity Manual (Rodegerdts 2007; Rodegerdts et al., 2007; TRB 2010), the mathematical form is $Q_e = Ae^{(-BQ_c)}$, in which $A = \frac{3600}{t_f}$ and $B = \frac{t_c - 0.5t_f}{3600}$. In the HCM6 edition, a lower value for t_c and t_f is suggested, but the mathematical equation remains the same (TRB 2016). Calibration of HCM model parameters can be found in (Wei and Grenard 2012; Gazzari et al., 2013; Mathew et al., 2017). A similar form can also be found in the Brilon-Wu model (Brilon et al., 1997; Wu 2001), which is used in the German Highway Capacity Manual, with $Q_e = 3600 \left(1 - \frac{\Delta Q_c}{l_e 3600}\right)^{l_e} \frac{l_c}{t_f} e^{-\frac{Q_c}{3600} (t_c - \frac{t_f}{2} - \Delta)}$, in which l_e and l_c represent the numbers of entry lanes and circulating lanes, and Δ is the intra-bunch minimum headway within each bunch in the circulating flow. The SR45 gap acceptance model (Troutbeck 1989) has a form of $Q_e = \frac{aQ_c e^{-\lambda(t_c - \Delta)}}{1 - e^{-\lambda t_f}}$, where a is the proportion of free vehicles with $a = 0.75(1 - \frac{\Delta v_c}{3600})$, and λ is a scale parameter or decay rate with $\lambda = \frac{av_c}{3600(1 - \frac{\Delta v_c}{3600})}$. A more generalized capacity formula for minor vehicles crossing or

merging into a major stream was proposed by Hagring (1998), $Q_e = \prod_i^{\alpha_i Q_{ci}} \frac{e^{-\sum_k \lambda_k t_{ck}}}{e^{-\Delta(1 - e^{-\sum_m \lambda_m t_{fm}})}}$, where \wedge is the summation of λ_i ; For i th lane of main stream, α_i is the proportion of free vehicles not driving in platoons; Q_{ci} is the circulating flow; λ_i is a decay constant; for k th lane of main stream, λ_k is the decay constant and t_{ck} is the critical gap; for m th lane of main stream, λ_m is the decay constant t_{fm} is the follow-up time; Δ is the minimum headway between two vehicles. This model could derive the entry capacity of multi-lane roundabout allowing different critical gaps, follow-up times and headway distributions including Cowan's M3 or exponential. This model can be generalized to be applied to estimating mixed traffic flow capacity on a shared entry lane of turbo-roundabout (Kociánová 2021). Additional research on a gap-acceptance model can also be found in (Akcelik 1994; Akcelik et al., 1998; Akçelik 2007; Xu and Tian 2008; Akçelik 2011; Fitzpatrick et al., 2013; Guo et al., 2019), as well as many others.

Despite the various forms being used, one general criticism of gap acceptance based models is that they do not directly quantify the relationship between geometry (the only factor which can be controlled by a roundabout designer) and capacity (Yap et al., 2013). In particular, a common strategy is to adopt a fixed value for a critical gap, as suggested by HCM6 or other references. Such a fixed value for a critical gap, however, when adopted, ignores the operating conditions of the roundabout. Calibration of a critical gap at each location, on the other hand, is labor-intensive and unrealistic. Other methods to assess the capacity of roundabout can also be found in the literature. For example, Krivda (2005) estimated roundabout entry capacity with original theory of uncontrolled intersections with the formula $Q_e = \frac{Q_c}{e^{Q_c * \frac{t_c}{3600}} - e^{Q_c * \frac{t_c - t_f}{3600}}}$, which was further proved to be comparable with other empirical and gap acceptance based models (Krivda and Petru 2018). Based on Tanner's formula that estimated capacity at an uncontrolled intersection (Tanner 1962), Fisk (1991) proposed a iterative method to derive roundabout capacity when all arms were saturated and flow conservation constraints were satisfied, which was similar as the reserve capacity estimation method by Wong (1996). Pollatschek et al. (2002) developed an unsignalized intersection capacity model as $Q_e = \int_a^{\infty} (\sum_{i=1}^{\infty} i p_i(\alpha) f(\alpha) d(\alpha))$ which could also be used to roundabout capacity estimation.

In this formula, α is a risk parameter that represents entering drivers' propensity to take a risk; i is the number of entering vehicles; $p_i(\alpha)$ is the probability that exactly i vehicles will enter a random gap in the major stream, consisting critical gap of individual vehicle t_{ci} and perceived average gap \bar{t}_f ; $f(\alpha)$ is the probability distribution function of α over all entering drivers. It is a microscopic model that considers individual preference by introducing individual critical gap. Bunker and Troutbeck (2003) further took limited priority

merging into consideration when calculating minor stream capacity by adding a limited priority term. However, these two methods still required calibration of critical gap and follow up headway. On the other hand, micro-simulation method was also adopted to predict entry capacity, and it was claimed to better illustrate the real conditions in traffic (Tollazzi et al., 2008; Krivda and Petru 2017). However, those simulation-based research were focused on the impact of pedestrian flow on the capacity instead of the entry capacity derivation (Fig 7).

In the next two sections, we first discuss the fundamentals of traffic dynamics, with a state-based analytical approach, and, then, analytically derive the roundabout capacity, based on the merging state transitions, and with variables that are easier to calibrate, including circulating speed, human perception response time, and vehicle performance.

3. Roundabout traffic dynamics analysis with a state-based analytical approach

In this section, we show how to analyze the traffic dynamics of a roundabout with a state-based analytical approach. We first extract the roundabout geometry into a Y-Shaped network, and illustrate the traffic movement with a state-space-time diagram. Then, we define episode, as well as a merging vehicle's state space. Finally, we draw state transition diagram by enumerating all possible state transition combinations. The goal of this section is to perform analytical analysis on the roundabout traffic dynamics, and to discuss its theoretical properties, which will contribute to the capacity derivation in the next section. It should be noted that the vehicle here denotes standard passenger car in a base condition. The notations used in this and the next sections are listed in Appendix A.

3.1. Geometry extraction as a Y-shaped network

We focus our analysis on a general one-lane roundabout, as shown in Fig. 1-a, with red vehicles representing entry flow Q_e , and blue vehicles representing circulating flow Q_c . Location C (the purple star) is the conflicting point between Q_e and Q_c , at the south entrance of the roundabout. Point A is an upstream location within the roundabout, point B is an upstream location on the roundabout entry leg, and point D is the downstream location within the roundabout. Vehicle arrivals are assumed to follow Poisson distribution. To effectively capture entry capacity, at least the analyzed entry approach (e.g., the South approach in Fig. 1) needs to be saturated during the analysis period. The other approaches may or may not be saturated.

Based on Fig. 1-a, we can extract the key roundabout geometry of interest, as well as the traffic movements, and simplify them as a Y-shaped network in Fig. 1-b. In Fig. 1-b, circulating flow Q_c drives from point A to point C, and entry flow Q_e drives from point B to point C. Q_e and Q_c intersect at point C. After merging at point C, Q_e and Q_c both drive towards downstream location D. Further, we add a single dummy node W to represent a vehicle waiting at point C. Due to the existence of a yield sign at point C, the entry vehicles need to give priority to the circulating traffic. As a result, traffic flow of arc BC will have to find an acceptance gap in the traffic flow of arc AC. If an acceptance gap is found, they will proceed to arc CD. Otherwise, they will have to wait at dummy point W (i.e., arc CW is the downstream arc), so the entry flow can wait at location W, until an acceptance gap shows up and, then, they will travel along arc WC back to point C, from which they will proceed to arc CD to move downstream. It is also straightforward to tell that no traffic flow is allowed from arc AC to arc CW.

3.2. Traffic movements illustration with state-space-time diagram

The network extraction and expansion in Fig. 1-b allow us to illustrate the traffic movements with a state-space-time diagram. In

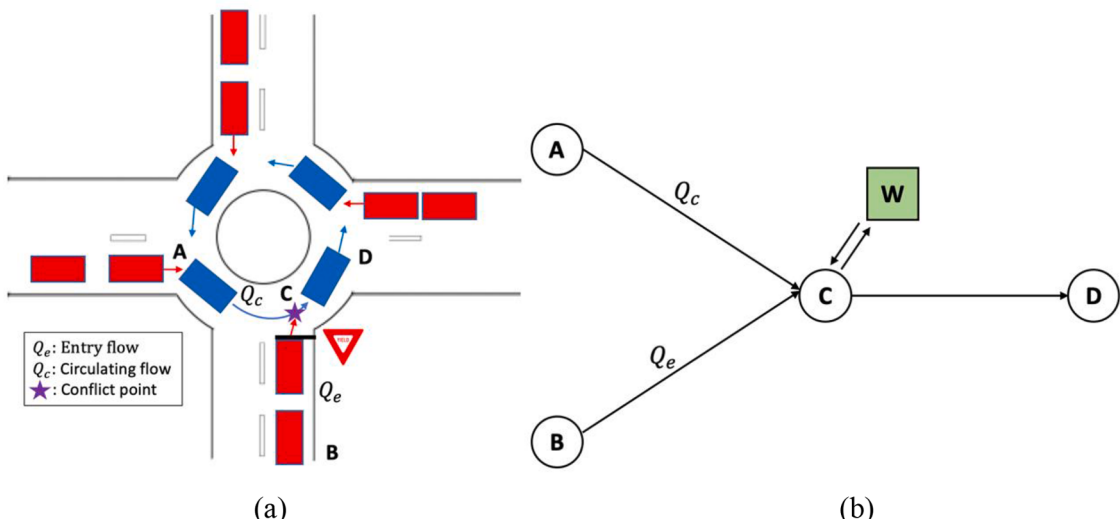


Fig. 1. Illustration of a typical roundabout. (a) Roundabout illustration, (b) Roundabout network extraction and expansion with dummy node.

Fig. 2 below, the X-axis is the time dimension, and the Y-axis represents the space. The five nodes, i.e., points A, B, C, D, and W are plotted on the Y axis. Due to the Y-shaped network geometry in **Fig. 1-b**, we separate arc AC from arc BC, and use green lines (e.g., lines EF and QP) to denote the vehicle trajectories along arc BC, i.e., the entry flow Q_e , and use blue lines (e.g., lines GH and UV) to denote the vehicle trajectories along arc AC, i.e., the circulating flow Q_c . We then use a black dashed vertical line (e.g., lines FJ and PQ) to connect the vehicle trajectory that arrives at point C through arc BC (e.g., line EF), with its subsequent trajectory that leaves point C for the downstream arcs (e.g., line JK). In this way, vehicles that arrive at point C from both arcs (AC and BC) can travel downstream to arc CD.

Next, we analyze the vehicle state at location C. The focus is placed on the entry vehicles (green lines). This is because the circulating vehicles (blue lines) have priorities, so there is no need for them to wait. It means that, from AC to CD, the blue lines can always go through without stopping. For example, line GH directly leads to line HI. However, the entry vehicles (green lines) are a bit tricky. When they arrive at location C, they need to first check the headway gap in the circulating flow. If the headway gap is sufficient, they will proceed to merging on to the roundabout, otherwise, they will have to wait for the next headway gap. As illustrated above in **Fig. 1-b**, when waiting happens, we use the dummy node W to represent the waiting behavior of the entry vehicle, i.e., we send the vehicle to arc CW. Later on, when an acceptance gap is observed, this waiting entry vehicle will travel along arc WC, back to location C, and finally merge into the roundabout.

For example, in **Fig. 2** above, the first entry vehicle EF arrives at point F (which is the same as point J), and the next circulating vehicle arrives at point H. The headway is thus JH, which is too short for the entry vehicle to merge into the roundabout. As a result, this entry vehicle has to stop and wait, and we use a red dashed vertical line JK to send this vehicle to the dummy location W. It will continue to wait there until point L, when the circulating vehicle GH has passed the conflicting location C. Then this entry vehicle can come back to location C, via another red dashed vertical line LM, and finally, merge into the roundabout by following green line MN. However, when the second entry vehicle (denoted as OP) arrives at the roundabout, the headway gap in the conflicting traffic is sufficiently high, so it can proceed to merging by following line QR, without waiting.

Further, we define an episode as the period of time between the arrivals of two consecutive circulating vehicles, at location C. For example, in **Fig. 2** above, blue line GH denotes the trajectory of the first circulating vehicle, and UV denotes that of the second circulating vehicle. They arrive at location C, at times H and V, respectively. So, we use point H as the start of the episode, and use point V as the end of the episode. Per definition of roundabout capacity, the entry flow is assumed to be saturated (otherwise we won't be able to observe the full capacity), whereas the circulating traffic may or may not be saturated. As such, the arrival rate along arc BC is higher than, or equal to, the arrival rate along arc AC. In other words, within one episode (e.g., HV), we may have multiple vehicles arriving at the roundabout from arc BC.

Fig. 2 also shows that the trajectory of the entry vehicles exhibits repeated patterns. At the beginning of an episode, a circulating vehicle arrives, so the entry vehicle has to stop and wait. Then, after a full stop, this entry vehicle accelerates and merges into the roundabout, and the following entry vehicles will continue to merge, without stopping. The episode ends when the next circulating

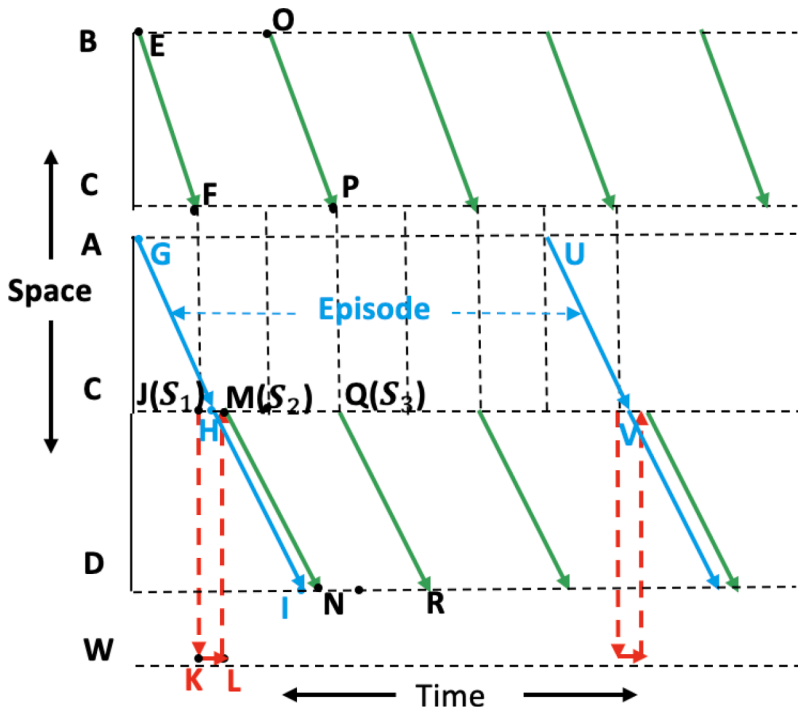


Fig. 2. State-space-time diagram of traffic movement.

vehicle arrives, which again interrupts the traffic flow and forces the merging vehicles to stop and wait. In other words, an episode always starts with an entry vehicle that experiences a full stop, followed by a platoon of succeeding vehicles and, finally, ends with another entry vehicle that experiences a full stop.

3.3. State space definition

In this subsection we define the state space of roundabout merging vehicles. We focus on the first entry vehicle in a queue, i.e., the head of an entry vehicle queue, and define the following three states $S = \{S_1, S_2, S_3\}$.

- 1 **Wait state S_1 :** the entry vehicle arrives at a roundabout but is unable to find an acceptable gap and, thus, is forced to wait at the stop line for the next allowable headway gap.
- 2 **Acceleration state S_2 :** an acceptable gap shows up, and the waiting vehicle accelerates to enter the roundabout with $v_e = 0$.
- 3 **Following state S_3 :** an acceptable gap is observed when the entry vehicle arrives, so it can follow its immediate leading vehicle to enter the roundabout with $0 < v_e \leq v_c$, without a need to come to a full stop. v_c is the circulating speed of the vehicles in the roundabout.

We visualize these three states of the entry vehicle (as shown below in Fig. 3), based on the same network abstraction in Fig. 1-b. The red dashed arcs denote the entry vehicles' movements, whereas the black arcs denote the network geometry. Fig. 3-a represents wait state S_1 , in which an acceptable gap is not available, so this entry vehicle has to travel to CW and wait at the dummy location W. When an acceptable gap shows up, the state of this vehicle becomes acceleration state S_2 , and it travels back to location C through arc WC, and then merges into the roundabout via arc CD (Fig. 3-b). For vehicles in following state S_3 , the vehicle does not experience a full stop, but directly merges into the roundabout, as illustrated in Fig. 3-c. The corresponding arcs for S_1, S_2, S_3 are AC and CW, WC and CD, and AC and CD, respectively.

Based on such definitions and state-arc mapping, we can see that point J in the state-space-time diagram in Fig. 2 has a state of S_1 , as the vehicle travels from arc AC to CW. Point M has a state of S_2 , as the vehicle travels from arc WC to CD, and point Q has a state of S_3 , as the vehicle travels from arc AC to CD.

3.4. State transition diagrams

We then analyze the transition between these three vehicle states and use state transition diagram to illustrate all possible transitions. A total of six possible state transition combinations can be enumerated, and we use Fig. 4 to illustrate their relationships.

We further describe each state transition below. Note that the study object is always the head of the entry vehicle queue, so if the first vehicle has merged on to the roundabout, the next vehicle in the queue becomes the head of the queue and, thus, becomes the new study object.

- 1 $S_1 \rightarrow S_1$: an entry vehicle has come to a full stop and, if an acceptable headway does not show up, it will have to continue to wait. No vehicle is able to enter the roundabout, and vehicles continue to queue up at the entrance.
- 2 $S_1 \rightarrow S_2$: an entry vehicle has come to a full stop and, when an acceptable headway shows up, it starts to accelerate to enter the roundabout. The number of vehicles that can enter the roundabout is one, and the speed of the entry vehicle is $v_e = 0$.
- 3 $S_2 \rightarrow S_1$: after the first fully-stopped vehicle merges into the roundabout, the remaining headway in the circulating flow is not sufficient for the second vehicle (which now becomes the first vehicle in the queue) to enter the roundabout and, as such, it is forced to stop. The number of vehicles that can enter the roundabout is one.
- 4 $S_2 \rightarrow S_3$: after the first fully-stopped vehicle merges into the roundabout, the remaining headway in the circulating flow is still sufficient for the second vehicle to enter and, as such, it can enter the roundabout at a speed of $v_e > 0$. The number of vehicles that can enter the roundabout is two.

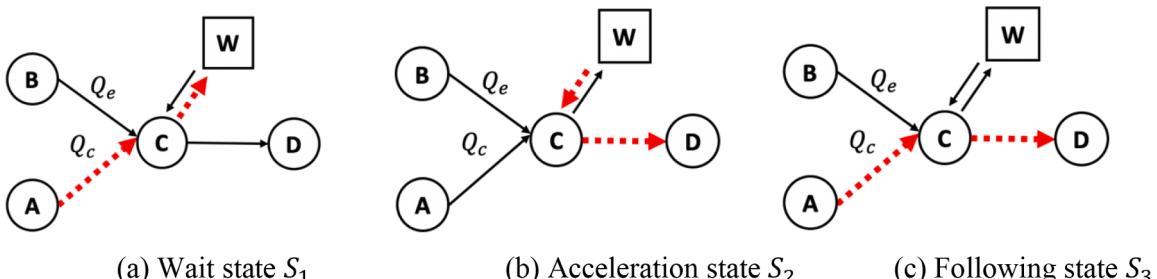


Fig. 3. Merging state definition of the first entry vehicle

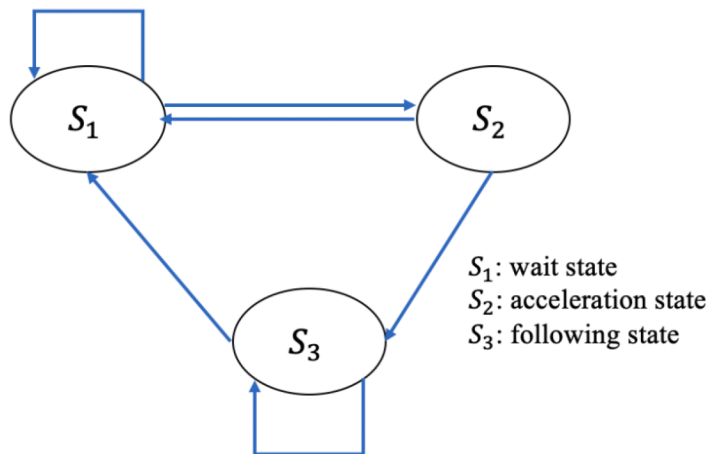


Fig. 4. State transition diagram of merging vehicles.

5 $S_3 \rightarrow S_1$: after the first vehicle merges into the roundabout with a state of S_3 , the remaining headway in the circulating flow is not sufficient for the second vehicle to enter and, as such, it is forced to stop and becomes the first vehicle in the queue. The number of vehicles that can enter the roundabout is one.

6 $S_3 \rightarrow S_3$: after the first vehicle merges into the roundabout with a state of S_3 , the remaining headway in the circulating flow is still sufficient for the second vehicle to enter and, as such, it can enter the roundabout at a speed of $v_e > 0$. The number of vehicles that can enter the roundabout is two.

It is easy to tell that per vehicle state definitions, the state transition from S_1 to S_3 is not possible, as the definition of S_3 requires that the vehicle not come to a full stop. In addition, S_3 cannot lead to S_2 , since the definition of S_2 requires that the vehicle start from zero speed, and S_2 cannot lead to S_2 either, for the same reason. As such, we summarize the state transitions and the underlying physical meanings in Table 1.

We further note that the vehicle state transitions exhibit Markov chain property, i.e., the state of a merging vehicle is only affected by the immediate leading state, but not the others. This is due to the merging states' definitions and the nature of vehicle kinematics, and is also evidenced by the complete list of state transition combinations in Table 1: a new state S' (represented by the columns in Table 1) is only affected by the existing state S (represented by the rows in Table 1), and is not impacted by any states further upstream.

4. Merging state transition-based analytical derivation of roundabout capacity

Based on the theoretical analysis and properties of the roundabout traffic dynamics above, in this section, we further present the analytical derivation of roundabout capacity, based on the entry vehicle's merging state transition. We start by deriving the state transition probabilities, followed by enumeration of episode-based state transition chain possibilities, and finally derive the roundabout capacity of a generic scenario under steady state, as well as a special scenario where all roundabout entrances are saturated.

4.1. State transition probability derivation

We follow the same notations as the literature, and use t_c to denote the critical gap of a roundabout. t_c is the minimum time headway in the circulating flow stream that an entering vehicle needs, in order to safely enter a roundabout. It includes two components, with $t_{c,lead}$ being the required time headway so that the entering vehicle does not crash into the vehicle ahead (i.e., the leading vehicle), and $t_{c,lag}$ being the required time headway so that the circulating vehicle behind (i.e., the lagging vehicle) does not crash into the entering vehicle. In other words, we have $t_c = t_{c,lead} + t_{c,lag}$. We denote the driver's perception response time as t_r , vehicle maximum deceleration

Table 1

All possible combinations of entry vehicle states.

S	S_1	S_2	S_3
$\setminus S'$			
S_1	A stopped vehicle continues to wait	A stopped vehicle accelerates and enters roundabout	Impossible
S_2	After a stopped vehicle enters roundabout, the next vehicle has to wait	Impossible	After a stopped vehicle enters roundabout, the next vehicle in queue enters without stop
S_3	After a vehicle enters roundabout without stop, the next vehicle has to wait	Impossible	Multiple vehicles enter roundabout in a platoon, without stop

as a (m/s^2), circulating speed as v_c , and the speed of entering vehicle i as $v_{e,i}$. It should be noted that $v_{e,i}$ is a variable that depends on the vehicle's sequence i in an episode, and is strictly non-decreasing. For the first vehicle in the queue ($i = 0$) that experiences a full stop and starts to accelerate to enter the roundabout, $v_{e,0} = 0$, and for the following vehicles that pass the roundabout consecutively, we will have $0 < v_{e,i} \leq v_{e,i+1} \leq v_c$.

Let's first look at wait state S_1 . To transition into acceleration state S_2 , the required time headway in the circulating flow has to be large enough for a fully-stopped vehicle to safely merge into the roundabout. Considering the requirement for crash avoidance, the critical time headway can be computed as $t_c = t_{c,lead} + t_{c,lag} = t_r + \frac{v_{e,0}}{a} + t_r + \frac{v_c}{a}$. Since $v_{e,0} = 0$ for an entry vehicle in acceleration state S_2 , this equation is further simplified as $t_c = 2t_r + \frac{v_c}{a}$. Therefore, the transition probabilities from state S_1 to S_1 and S_2 can be derived as Eq. (1) and Eq. (2), respectively.

$$P(S_1 / S_1) = \int_0^{2t_r + \frac{v_c}{a}} \lambda e^{-\lambda t} dt = 1 - e^{-\lambda * \left(2t_r + \frac{v_c}{a}\right)} \quad (1)$$

$$P(S_2 / S_1) = 1 - P(S_1 / S_1) = e^{-\lambda * \left(2t_r + \frac{v_c}{a}\right)} \quad (2)$$

In which $\lambda = Q_c/3600$. As discussed before, we have $P(S_3 / S_1) = 0$.

Next, we look at acceleration state S_2 . Now that the first vehicle is able to merge into roundabout (per definition of acceleration state S_2), the next vehicle in the queue now becomes the new leading vehicle to examine. For state S_2 to transition to following state S_3 , the time headway should be sufficient for both vehicles to pass. In other words, the required time headway becomes $t_r + \frac{v_{e,0}}{a} + t_r + \frac{v_c}{a} +$

$t_r + \frac{v_{e,1}}{a} = 3t_r + \frac{v_c}{a} + \frac{v_{e,1}}{a}$. So, we have $P(S_2 \cap S_3) = \int_{3t_r + \frac{v_c}{a} + \frac{v_{e,1}}{a}}^{\infty} \lambda e^{-\lambda t} dt$. In addition, as evidenced in Fig. 4, the only state that may lead to S_2 is

S_1 , so we have $P(S_2) = P(S_2 / S_1)$ which is given in Eq. (2).

The transition probabilities from state S_2 to S_3 and S_1 can then be derived as Eq. (3) and Eq. (4), respectively.

$$P(S_3 / S_2) = \frac{P(S_2 \cap S_3)}{P(S_2)} = \frac{\int_{3t_r + \frac{v_c}{a} + \frac{v_{e,1}}{a}}^{\infty} \lambda e^{-\lambda t} dt}{\int_{2t_r + \frac{v_c}{a}}^{\infty} \lambda e^{-\lambda t} dt} = \frac{-e^{-\lambda * (\infty)} - (-e^{-\lambda * (3t_r + \frac{v_c}{a} + \frac{v_{e,1}}{a})})}{-e^{-\lambda * (\infty)} - (-e^{-\lambda * (2t_r + \frac{v_c}{a})})} = e^{-\lambda * \left(t_r + \frac{v_{e,1}}{a}\right)} \quad (3)$$

$$P(S_1 / S_2) = 1 - P(S_3 / S_2) = 1 - e^{-\lambda * \left(t_r + \frac{v_{e,1}}{a}\right)} \quad (4)$$

In which $0 < v_{e,1} \leq v_c$, and as discussed before, we have $P(S_2 / S_2) = 0$.

Finally, let's look at following state S_3 , which is a bit trickier. As S_3 may lead to another S_3 state, a platoon of vehicles may merge into the roundabout consecutively (i.e., with the first vehicle in acceleration state S_2 and all following vehicles in following state S_3). In other words, we may have multiple vehicles merging on to the roundabout, all in following state S_3 . The corresponding merging state chain is $S_1 \rightarrow S_2 \rightarrow S_3 \rightarrow \dots \rightarrow S_3$. Assume a platoon of n vehicles have merged on to the roundabout, with $n \geq 3$, the required headways is $t_r + \frac{v_{e,0}}{a} + t_r + \frac{v_c}{a} + (n-1) * t_r + \sum_{i=1}^{n-1} \frac{v_{e,i}}{a} = (n+1) * t_r + \frac{v_c}{a} + \sum_{i=1}^n \frac{v_{e,i}}{a}$. On the other hand, for a new vehicle (i.e., the $(n+1)^{th}$ vehicle in the queue) to also be able to merge into the roundabout, without experiencing a full-stop, the required headways is $t_r + \frac{v_{e,0}}{a} + t_r + \frac{v_c}{a} + n * t_r + \sum_{i=1}^n \frac{v_{e,i}}{a} = (n+2) * t_r + \frac{v_c}{a} + \sum_{i=1}^n \frac{v_{e,i}}{a}$.

Therefore, the transition probabilities from state S_3 to S_3 and S_1 can be derived as Eq. (5) and Eq. (6), respectively.

$$P(S_3 / S_3) = \frac{\int_{(n+2)*t_r + \frac{v_c}{a} + \sum_{i=1}^n \frac{v_{e,i}}{a}}^{\infty} \lambda e^{-\lambda t} dt}{\int_{(n+1)*t_r + \frac{v_c}{a} + \sum_{i=1}^{n-1} \frac{v_{e,i}}{a}}^{\infty} \lambda e^{-\lambda t} dt} = \frac{-e^{-\lambda * (\infty)} - (-e^{-\lambda * ((n+2)*t_r + \frac{v_c}{a} + \sum_{i=1}^n \frac{v_{e,i}}{a})})}{-e^{-\lambda * (\infty)} - (-e^{-\lambda * ((n+1)*t_r + \frac{v_c}{a} + \sum_{i=1}^{n-1} \frac{v_{e,i}}{a})})} = e^{-\lambda * \left(t_r + \frac{v_{e,n}}{a}\right)} \quad (5)$$

$$P(S_1 / S_3) = 1 - P(S_3 / S_3) = 1 - e^{-\lambda * \left(t_r + \frac{v_{e,n}}{a}\right)} \quad (6)$$

In which $0 < v_{e,n} \leq v_c$ and, as discussed before, we have $P(S_2 / S_3) = 0$.

4.2. Episode-based state transition chains analysis

As illustrated in Fig. 2 and in the associated discussion, an episode is defined by the time interval between the arrivals of two circulating vehicles, and the states of the entry vehicles exhibit repeated patterns. An episode always starts with an entry vehicle that experiences a full stop (i.e. wait state S_1), followed by a platoon of succeeding vehicles in acceleration state S_2 and following state S_3

and, finally, ends with another entry vehicle that experiences a full stop (i.e., S_1). In other words, an episode always starts, as well as ends, with a fully stopped vehicle. The number of vehicles in the platoon may be zero, i.e., no vehicle is able to merge into roundabout in an episode, or there could be multiple, depending on the duration of the available headway gap of the circulating traffic.

Based on these properties, we enumerate all state transition chain categories within one episode, and calculate their probabilities. We start from a low headway, when no vehicle can enter the roundabout, and gradually increase it to allow more vehicles to merge. In total, there are four different categories that we discuss below.

Entry vehicle pattern 1: no vehicle is able to enter the roundabout in an episode

When no vehicle is able to merge into a roundabout, the corresponding state transition chain is $S_1 \rightarrow S_1$. The probability is $P(S_1 \rightarrow S_1) = P(S_1) * P(S_1 / S_1) = 1 - e^{-\lambda * (2t_r + \frac{v_c}{a})}$. This is because, per discussion above, an episode always starts with a S_1 vehicle, so for the first vehicle, we have $P(S_1) = 1$, and $P(S_1 / S_1)$ is given in Eq. (1). For this scenario, no vehicle can merge, so the merging vehicles have to stop and wait.

Entry vehicle pattern 2: exactly one vehicle can enter the roundabout in an episode

When only one vehicle is able to merge into the roundabout, the corresponding state transition chain is $S_1 \rightarrow S_2 \rightarrow S_1$. The probability is $P(S_1 \rightarrow S_2 \rightarrow S_1) = P(S_1 \rightarrow S_2) * P(S_2 \rightarrow S_1) = P(S_1) * P(S_2 / S_1) * P(S_1 / S_2) = e^{-\lambda * (2t_r + \frac{v_c}{a})} * (1 - e^{-\lambda * (t_r + \frac{v_e}{a})}) = e^{-\lambda * (2t_r + \frac{v_c}{a})} - e^{-\lambda * (3t_r + \frac{v_c + v_{e,1}}{a})}$. For this scenario, only one vehicle can merge with S_2 state.

Entry vehicle pattern 3: exactly two vehicles can enter the roundabout in an episode

When exactly two vehicles are able to merge into the roundabout, the corresponding state transition chain is $S_1 \rightarrow S_2 \rightarrow S_3 \rightarrow S_1$. The probability is $P(S_1 \rightarrow S_2 \rightarrow S_3 \rightarrow S_1) = P(S_1 \rightarrow S_2) * P(S_2 \rightarrow S_3) * P(S_3 \rightarrow S_1) = e^{-\lambda * (2t_r + \frac{v_c}{a})} * e^{-\lambda * (t_r + \frac{v_{e,1}}{a})} * (1 - e^{-\lambda * (t_r + \frac{v_{e,2}}{a})}) = e^{-\lambda * (3t_r + \frac{v_c + v_{e,1}}{a})} - e^{-\lambda * (4t_r + \frac{v_c + v_{e,1} + v_{e,2}}{a})}$. For this scenario, two vehicles can merge, one in state S_2 and one in S_3 .

Entry vehicle pattern 4: more than two vehicles can enter the roundabout in an episode

When n vehicles are able to merge into the roundabout, with $n > 2$, the corresponding state transition chain is $S_1 \rightarrow S_2 \rightarrow S_3 \rightarrow \dots \rightarrow S_n \rightarrow S_1$. For this scenario, the first vehicle will merge in state S_2 , and the remaining $n - 1$ vehicles will merge in state S_3 . The length of this state transition chain can be as long as the headway gap allows. The probability of this state transition chain is derived in Eq. (7). For detailed derivation, please refer to Appendix-B.

$$\begin{aligned} P(S_1 \rightarrow S_2 \rightarrow S_3 \rightarrow \dots \rightarrow S_n \rightarrow S_1) &= P(S_1 \rightarrow S_2) * P(S_2 \rightarrow S_3) * P(S_3 \rightarrow S_4) * \dots * P(S_{n-1} \rightarrow S_n) * P(S_n \rightarrow S_1) \\ &= e^{-\lambda * \left((n+1)*t_r + \frac{v_c + \sum_{i=1}^{n-1} v_{e,i}}{a} \right)} - e^{-\lambda * \left((n+2)*t_r + \frac{v_c + \sum_{i=1}^n v_{e,i}}{a} \right)} \end{aligned} \quad (7)$$

Interestingly, we note that Eq. (7) is also generically applicable to categories 2 and 3, with $n = 1$ and $n = 2$. To prove this, plug in $n = 1$ and $n = 2$ to Eq. (7), and the results are the same as $P(S_1 \rightarrow S_2 \rightarrow S_1)$ and $P(S_1 \rightarrow S_2 \rightarrow S_3 \rightarrow S_1)$, respectively. As such, in the sections below, we will use Eq. (7) as the generic form of state transition chain probability to derive roundabout capacity.

4.3. Capacity derivation of generic scenario under steady state

In this subsection, we derive the roundabout capacity of a generical scenario, by finding solution of state transition under steady states. Here, we assume that in a generic scenario, at least the target entry approach is saturated, and the other entry approaches may or may not be saturated. This assumption is consistent with the other popular models, such as HCM. In contrast to this generic scenario, if all entry approaches are saturated, this problem becomes a special scenario with additional constraints, and is analyzed in the next section.

Given the relationship between state transition chains and the number of vehicles that can merge into the roundabout in each category, we can analytically calculate the number of vehicles that can enter a roundabout in an episode. For a period of time T , as the roundabout circulating flow rate is Q_c , the total number of headways in this period is $T * Q_c$. Here, we consider the base scenario that consists of only standard passenger cars. If heavy vehicles exist in circulating flow, they need to be converted to passenger cars via passenger car equivalency (PCE) factors. Learning from HCM6, $Q_c = Q_{c,veh} * (1 + P_T(E_T - 1))$, where Q_c and $Q_{c,veh}$ are circulating flow in pc/h and veh/h respectively; P_T is the proportion of heavy vehicles; E_T is the passenger car equivalent for heavy vehicles (i.e., 2 as suggested by HCM6). Therefore, the number of vehicles that may enter the roundabout thus becomes a function of T , Q_c , and v_c and v_e . With the generic state transition chain expression in Eq. (7), we have:

$$\begin{aligned} N(T, Q_c, v_c, v_e) &= T * Q_c * 0 * \left(1 - e^{-\lambda * \left(2t_r + \frac{v_c}{a} \right)} \right) + \sum_{n=1}^{\infty} n * \left(e^{-\lambda * \left((n+1)*t_r + \frac{v_c + \sum_{i=1}^{n-1} v_{e,i}}{a} \right)} - e^{-\lambda * \left((n+2)*t_r + \frac{v_c + \sum_{i=1}^n v_{e,i}}{a} \right)} \right) \\ &= T * Q_c * \sum_{n=1}^{\infty} n * \left(e^{-\lambda * \left((n+1)*t_r + \frac{v_c + \sum_{i=1}^{n-1} v_{e,i}}{a} \right)} - e^{-\lambda * \left((n+2)*t_r + \frac{v_c + \sum_{i=1}^n v_{e,i}}{a} \right)} \right) \end{aligned}$$

As discussed above, if the headway h in the roundabout traffic flow is sufficient for multiple vehicles to merge, we have $v_{e,0} = 0$ for

the first vehicle, and the entering speed is strictly non-decreasing for the following vehicles, with $0 < v_{e,i} \leq v_{e,i+1} \leq v_c$. The literature suggested various headway patterns for a platoon of vehicles that pass an intersection sequentially. For example, Jin et al. (2009) suggested that the position of the critical vehicle of a stable headway begins from 4 to 9 s, or after 10 to 14 s. HCM recommends that the calculation of saturation flow rate begins after the fifth vehicle. Hao and Ma (2017) performed a statistical test and found that the steady-flow headway begin with the fourth to fifth vehicle. Here we follow the HCM method, and assume the entering speed of the fifth vehicle would reach v_c when passing the stop line, i.e., $v_{e,5} = v_c$. Considering that roundabouts are geometrically designed, with relatively low operating speeds (e.g., 15–30 km/hr), this assumption should hold. Note that vehicles may still be required to decelerate from roadway operating speed, which could be much higher than v_c , to safely pass the roundabout. We use a linear interpolation method to approximate the entering speed of the i^{th} vehicles, i.e. $v_{e,i} = \frac{v_c}{5} * i$ for $1 \leq i \leq 5$, and $v_{e,i} = v_c$ for $i > 5$, or, $v_{e,i} = \frac{v_c}{5} * \min(i, 5)$ when combined.

$N(T, Q_c, v_c, v_e)$ can then be broken down into two components. We use $N_1(T, Q_c, v_c, v_e)$ and $N_2(T, Q_c, v_c, v_e)$ to denote the first and the second component, respectively, so that

$$N(T, Q_c, v_c, v_e) = N_1(T, Q_c, v_c, v_e) + N_2(T, Q_c, v_c, v_e) \quad (8)$$

$$N_1(T, Q_c, v_c, v_e) = T * Q_c * \sum_{n=1}^5 n * \left(e^{-\lambda * \left((n+1)*t_r + \frac{v_c + \sum_{i=1}^{n-1} v_{e,i}}{a} \right)} - e^{-\lambda * \left((n+2)*t_r + \frac{v_c + \sum_{i=1}^n v_{e,i}}{a} \right)} \right) \quad (9)$$

$$N_2(T, Q_c, v_c, v_e) = T * Q_c * \sum_{n=6}^{\infty} n * \left(e^{-\lambda * \left((n+1)*t_r + \frac{v_c + \sum_{i=1}^{n-1} v_{e,i}}{a} \right)} - e^{-\lambda * \left((n+2)*t_r + \frac{v_c + \sum_{i=1}^n v_{e,i}}{a} \right)} \right) \quad (10)$$

Let us first look at $N_1(T, Q_c, v_c, v_e)$. We notice that, when the equation of $N_1(T, Q_c, v_c, v_e)$ is fully expanded, some items will be canceled out. $N_1(T, Q_c, v_c, v_e)$ is then reformulated as Eq. (11). For a detailed derivation, please refer to Appendix B.

$$N_1(T, Q_c, v_c, v_e) = T * Q_c * \left[e^{-\lambda * \left(2*t_r + \frac{v_c}{a} \right)} + e^{-\lambda * \left(3*t_r + \frac{6*v_c}{5*a} \right)} + e^{-\lambda * \left(4*t_r + \frac{8*v_c}{5*a} \right)} + e^{-\lambda * \left(5*t_r + \frac{11*v_c}{5*a} \right)} + e^{-\lambda * \left(6*t_r + 3*\frac{v_c}{a} \right)} - 5e^{-\lambda * \left(7*t_r + 4*\frac{v_c}{a} \right)} \right] \quad (11)$$

Then, we look at $N_2(T, Q_c, v_c, v_e)$. Similarly, when all items in Eq. (10) are expanded, some items are canceled out. Then $N_2(T, Q_c, v_c, v_e)$ is reformulated as Eq. (12). For a detailed derivation, please refer to Appendix B.

$$N_2(T, Q_c, v_c, v_e) = T * Q_c * \left[6 * e^{-\lambda * \left(7*t_r + \frac{4*v_c}{a} \right)} + \lim_{N \rightarrow \infty} \sum_{i=6}^{N-1} e^{-\lambda * \left((i+2)*t_r + \frac{(i-1)*v_c}{a} \right)} - \lim_{N \rightarrow \infty} N e^{-\lambda * \left((N+2)*t_r + \frac{(N-1)*v_c}{a} \right)} \right] \quad (12)$$

Plug in $N_1(T, Q_c, v_c, v_e)$ and $N_2(T, Q_c, v_c, v_e)$ from Eqs. (11) and (12) into Eq. (8), and we can get Eq. (13) below.

$$N(T, Q_c, v_c, v_e) = T * Q_c * \left[e^{-\lambda * \left(2*t_r + \frac{v_c}{a} \right)} + e^{-\lambda * \left(3*t_r + \frac{6*v_c}{5*a} \right)} + e^{-\lambda * \left(4*t_r + \frac{8*v_c}{5*a} \right)} + e^{-\lambda * \left(5*t_r + \frac{11*v_c}{5*a} \right)} + e^{-\lambda * \left(6*t_r + 3*\frac{v_c}{a} \right)} \right. \\ \left. + \lim_{N \rightarrow \infty} \sum_{i=5}^{N-1} e^{-\lambda * \left((i+2)*t_r + \frac{(i-1)*v_c}{a} \right)} - \lim_{N \rightarrow \infty} N e^{-\lambda * \left((N+2)*t_r + \frac{(N-1)*v_c}{a} \right)} \right] \quad (13)$$

It is easy to tell that $\sum_{i=5}^{N-1} e^{-\lambda * \left((i+2)*t_r + \frac{(i-1)*v_c}{a} \right)}$ is a geometric sequence, so that the summation can be computed as $\lim_{N \rightarrow \infty} \sum_{i=5}^{N-1} e^{-\lambda * \left((i+2)*t_r + \frac{(i-1)*v_c}{a} \right)} = \frac{e^{-\lambda * \left(7*t_r + \frac{4*v_c}{a} \right)}}{1 - e^{-\lambda * \left(t_r + \frac{v_c}{a} \right)}}$. With regard to the last item, $\lim_{N \rightarrow \infty} N e^{-\lambda * \left((N+2)*t_r + \frac{(N-1)*v_c}{a} \right)} = \lim_{N \rightarrow \infty} \frac{N}{e^{\lambda * \left((N+2)*t_r + \frac{(N-1)*v_c}{a} \right)}} = 0$. For a detailed derivation, please refer to Appendix B.

As $\lambda = Q_c/3600$, and $Q_e = \frac{N(T, Q_c, v_c, v_e)}{T}$, we can further reformulate Eq. (13) to compute the roundabout capacity $Q_e = Q_c * \left[e^{-\frac{Q_c}{3600} * (2*t_r + \frac{v_c}{a})} + e^{-\frac{Q_c}{3600} * (3*t_r + \frac{6*v_c}{5*a})} + e^{-\frac{Q_c}{3600} * (4*t_r + \frac{8*v_c}{5*a})} + e^{-\frac{Q_c}{3600} * (5*t_r + \frac{11*v_c}{5*a})} + e^{-\frac{Q_c}{3600} * (6*t_r + \frac{15*v_c}{5*a})} + \frac{e^{-\frac{Q_c}{3600} * (7*t_r + 4*\frac{v_c}{a})}}{1 - e^{-\frac{Q_c}{3600} * (t_r + \frac{v_c}{a})}} \right]$.

If we use τ_i to denote the required headway gap for a total of i entry vehicles to safely merge into the roundabout, the roundabout capacity Q_e in pc/h becomes:

$$Q_e = Q_c * \left(\sum_{i=1}^5 e^{-\frac{Q_c}{3600} * \tau_i} + \frac{e^{-\frac{Q_c}{3600} * \tau_6}}{1 - e^{-\frac{Q_c}{3600} * (\tau_1 + \frac{v_c}{a})}} \right) \quad (14)$$

In which $\tau_1 = 2 * t_r + \frac{v_c}{a}$, $\tau_2 = 3 * t_r + \frac{v_c}{a} * \frac{6}{5}$, $\tau_3 = 4 * t_r + \frac{v_c}{a} * \frac{8}{5}$, $\tau_4 = 5 * t_r + \frac{v_c}{a} * \frac{11}{5}$, $\tau_5 = 6 * t_r + \frac{v_c}{a} * \frac{15}{5}$, and $\tau_6 = 7 * t_r + 4 * \frac{v_c}{a}$.

Based on Eq. (14), it can be found that the key inputs to roundabout capacity calculation are circulating flow rate Q_c , which is consistent with the gap-acceptance model, as well as circulating speed v_c , human perception response time t_r , and vehicle braking performance a . We note that v_c , not only allows us to calculate the critical gap t_c when combined with t_r and a , but also reflects the

conditions of operation that are specifically related with the roundabout of interest. For example, many design factors, such as roundabout radius, lane width, speed limit, and grading, all impact a vehicle's circulating speed inside a roundabout v_c . Further, the calibration of circulating speed v_c is not difficult with existing data sources, as partial trajectory data from a portion of vehicles, e.g., collected from smartphone devices or connected vehicles, or collected by drones just like the case study of this manuscript, is sufficient for circulating speed calibration.

4.4. Capacity derivation with all entrances being saturated

In this section, we discuss the special scenario with all four approaches to the roundabout being saturated. This scenario deems special attention, due to the interrelationship between Q_e and Q_c . For example, the entry flow at southern entrance $Q_{e,S}$ becomes part of the circulating flow of the eastern entrance $Q_{e,E}$, thus affecting the Q_e of eastern entrance $Q_{e,E}$ which, in turn, becomes part of the circulating flow of the southern entrance $Q_{e,S}$, and affects the Q_e of the southern entrance $Q_{e,S}$. In other words, the Q_e and Q_c , located on the left and right side of Eq. (14), respectively, are now interrelated. Note that such $Q_e \sim Q_c$ relationship only holds when all roundabout approaches are saturated. Otherwise, the entry flow rate is lower than capacity Q_e , and it becomes problematic to use Q_e to denote the flow rate of entry vehicles.

Assume that a vehicle gets off at the next immediate exit with a probability of p_1 , at a second exit with p_2 , at a third exit with p_3 , and at the last exit with p_4 . We shall have $p_1 + p_2 + p_3 + p_4 = 1$. For simplicity, we assume a symmetric roundabout with homogenous traffic flow, i.e., the values of p_1, p_2, p_3, p_4 remain the same, regardless of which entry approach is used. In addition, in a symmetric roundabout, the circulating speed is the same for all four entry approaches and, thus, when saturated, all four approaches will have equal entry capacity, i.e., $Q_{e,S} = Q_{e,E} = Q_{e,N} = Q_{e,W} = Q_e$. With this (as shown in Fig. 1-a), in a symmetric saturated roundabout with vehicles waiting at all four approaches, the circulating flow rate at the conflict point can be derived as Eq. (15).

$$Q_c = Q_{e,W} * (p_2 + p_3 + p_4) + Q_{e,N} * (p_3 + p_4) + Q_{e,E} * (p_4) = Q_e * (p_2 + 2p_3 + 3p_4) \quad (15)$$

To simplify the mathematical form, we define traffic circulating index β as Eq. (16) below and, then, with β , Eq. (15) could be transformed as Eq. (17)

$$\beta = p_2 + 2p_3 + 3p_4 \quad (16)$$

$$Q_c = Q_e * \beta \quad (17)$$

β quantitatively defines the spatial demand distribution, or, the average travel distance within the roundabout. If the average travel distance is low, for example, most vehicles exit the roundabout from the first exit, β value will decrease, and so will Q_c , even if traffic demand Q_e remains unchanged. On the other hand, when the average travel distance increases, for example, when the ratio of vehicles exiting the roundabout from the second and third exits increases, the β value will increase, and so will Q_c . In this way, we can trace the vehicles in a circulating flow back to the entry flow.

Plugging Eq. (17) into Eq. (14), we will obtain Eq. (18) below that allows us to find a solution for capacity Q_e , when all four approaches are saturated.

$$\beta * \left[\sum_{i=1}^5 e^{-\frac{Q_e}{3600} * \beta * \tau_i} + \frac{e^{\frac{Q_e}{3600} * \beta * \tau_6}}{1 - e^{-\frac{Q_e}{3600} * \beta * (\tau_r + \frac{v_c}{a})}} \right] - 1 = 0 \quad (18)$$

In Eq. (18), Q_e is the dependent variable to solve. Roundabout circulating speed v_c , and traffic circulating index β are two independent variables. Driver response time τ_r , vehicle max deceleration value a are the input parameters. In other words, Eq. (18) can be expressed as $Q_e = f(v_c, \beta; \tau_r, a)$. To show that Eq. (18) has a unique solution, we introduce an auxiliary function $g(Q_e)$, and make it equal to the left side of Eq. (18), i.e., $g(Q_e) = \beta * \left[\sum_{i=1}^5 e^{-\frac{Q_e}{3600} * \beta * \tau_i} + \frac{e^{\frac{Q_e}{3600} * \beta * \tau_6}}{1 - e^{-\frac{Q_e}{3600} * \beta * (\tau_r + \frac{v_c}{a})}} \right] - 1$.

The first-order derivative $g'(Q_e)$, is derived and proven to be negative, i.e., $g'(Q_e) < 0$, which means $g(Q_e)$ is monotonically decreasing. For detailed derivation, please refer to Appendix B. With $g(Q_e)$ strictly decreasing, we only need to show that, if there exists a solution for $g(Q_e) = 0$, the solution must be unique.

When Q_e takes a very small value that is close to zero:

$$\lim_{Q_e \rightarrow 0} \frac{e^{-Q_e * \beta * \tau_6}}{1 - e^{-Q_e * \beta * (\tau_r + \frac{v_c}{a})}} = \lim_{Q_e \rightarrow 0} \frac{1}{e^{Q_e * \beta * (7 * \tau_r + 4 * \frac{v_c}{a})} - e^{Q_e * \beta * (6\tau_r + 3 * \frac{v_c}{a})}} = +\infty$$

While the other items of $g(Q_e)$, i.e., $e^{-Q_e * \beta * \tau_i}$, are equal to 1 and, thus, $\lim_{Q_e \rightarrow 0} g(Q_e) = +\infty$.

On the other hand, when Q_e takes a very high value:

$$\lim_{Q_e \rightarrow \infty} \frac{e^{-Q_e * \beta * \tau_6}}{1 - e^{-Q_e * \beta * (\tau_r + \frac{v_c}{a})}} = \lim_{Q_e \rightarrow \infty} \frac{1}{e^{Q_e * \beta * (7 * \tau_r + 4 * \frac{v_c}{a})} - e^{Q_e * \beta * (6\tau_r + 3 * \frac{v_c}{a})}} = 0$$

And the other items of $g(Q_e)$ all equal to 0 and, thus, $\lim_{Q_e \rightarrow \infty} g(Q_e) = -1$.

To summarize, since we have $\lim_{Q_e \rightarrow 0} g(Q_e) * \lim_{Q_e \rightarrow \infty} g(Q_e) < 0$, and $g'(Q_e) < 0$, there exists a unique solution to $g(Q_e) = 0$.

Next, we use Newton's method, a classic root-finding algorithm to iteratively approximate the root of function $g(Q_e) = 0$. The basic idea is to start with an initial guess, which may or may not be close to the true root, then approximate the function by its tangent line using first derivative $g'(Q_c)$ and, finally, compute the x-intercept of this tangent line. This x-intercept will typically be a better approximation of the original function's root than the first guess, and the method is iterated until the error is within a certain acceptable range. The pseudo of the root-finding algorithm is given below.

Root-finding algorithm to approximate roundabout capacity Q_e

1. Start
 2. Input
 - a. Target function $g(Q_e)$
 - b. Derivative of target function $g'(Q_e)$
 - c. Initialize an initial guess $Q_{e,old}$
 - d. Define a tolerable error threshold err
 3. Find a new guess $Q_{e,new} = Q_{e,old} - g(Q_{e,old})/g'(Q_{e,old})$
 4. If $abs(g(Q_{e,new})) < err$, return $Q_{e,new}$ as solution; else go to step 5
 5. $Q_{e,old} = Q_{e,new}$, go to step 3 and iterate
 6. End
-

4.5. Capacity derivation of multilane scenario

In this section, we discuss the multilane roundabout capacity for two-lane entries conflicted by two circulating lanes. The derivation is also based on the merging state transition and is an extension of the single lane scenario. As illustrated in Fig. 5, there are two entry flows conflicted by two conflicting flows for Approach 1. We use superscript O to denote outer circulating lane, I for inner circulating lane, and L and R for left entry lane and right entry lane, respectively. The entry capacity is the summation of the left lane capacity Q_e^L and right lane capacity Q_e^R , i.e., $Q_e^M = Q_e^L + Q_e^R$. Since Q_e^R can be computed with Eq. (14), in this subsection we will focus on the derivation of Q_e^L , which conflicts with both circulating flow Q_c^I and Q_c^O , on the inner and outer lane, respectively.

For the derivation of Q_e^L , let's also start from state transition probability derivation. For the wait state S_1 to transition into acceleration state S_2 , acceptable gaps need to be observed on both left lane and right lane simultaneously. The critical headway for the outer circulating lane is $t_c^O = t_{c,lead}^O + t_{c,lag}^O = t_r + \frac{v_{c,0}^O}{a} + t_r + \frac{v_c^O}{a} = 2t_r + \frac{v_c^O}{a}$, and the critical headway for the inner circulating lane is $t_c^I = t_{c,lead}^I + t_{c,lag}^I = t_r + \frac{v_{c,0}^I}{a} + t_r + \frac{v_c^I}{a} = 2t_r + \frac{v_c^I}{a} + \frac{v_c^O}{a}$. Hence, the transition probabilities from state S_1 to S_2 becomes the product of the probability of headway higher than critical headway on both lanes. $P^L(S_2 / S_1) = \int_{2t_r + \frac{v_c^O}{a}}^{\infty} \lambda^O e^{-\lambda^O t} dt * \int_{2t_r + \frac{v_c^I + v_c^O}{a}}^{\infty} \lambda^I e^{-\lambda^I t} dt = e^{-\lambda^O * (2t_r + \frac{v_c^O}{a})} - \lambda^I * (2t_r + \frac{v_c^O + v_c^I}{a})$, and similarly $P^L(S_1 / S_1) = 1$

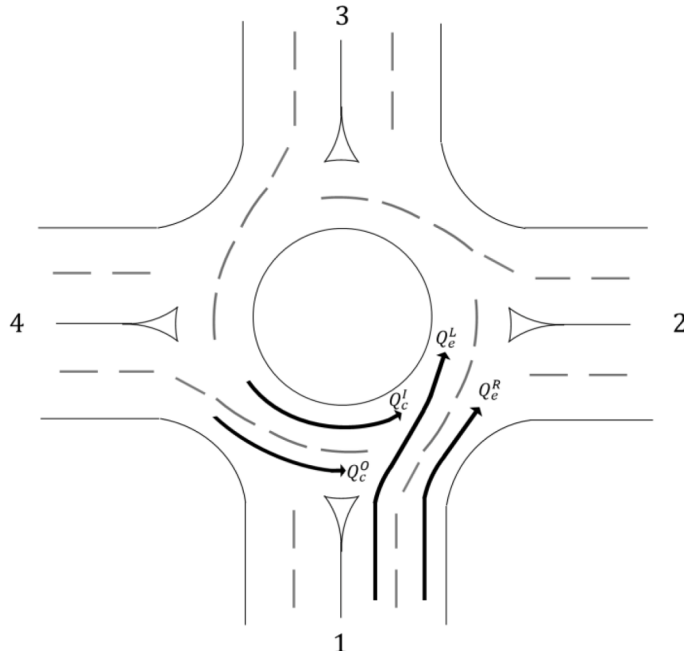


Fig. 5. Example of two-lane entry conflicted by two circulating lanes.

$-P^L(S_2/S_1) = 1 - e^{-\lambda^O * \left(2t_r + \frac{v_c^O}{a}\right) - \lambda^I * \left(2t_r + \frac{v_c^O + v_e^I}{a}\right)}$, in which $\lambda^O = Q_c^O/3600$, $\lambda^I = Q_c^I/3600$. Also, we have $P^L(S_3/S_1) = 0$. Then when it comes to acceleration state S_2 , if transits to following state S_3 , the time headway of both outer and inner circulating lane should allow two vehicles to merge in. The critical time headways are $t_r + \frac{v_{e,0}^O}{a} + t_r + \frac{v_c^O}{a} + t_r + \frac{v_{e,1}^O}{a} = 3t_r + \frac{v_c^O}{a} + \frac{v_{e,1}^O}{a}$, and $t_r + \frac{v_{e,0}^I}{a} + t_r + \frac{v_e^I}{a} + t_r + \frac{v_{e,1}^I}{a} = 3t_r + \frac{2v_c^O}{a} + \frac{v_e^I}{a}$, respectively., and as discussed in single lane case, $P^L(S_2/S_2) = 0$.

For following state S_3 , for the merging state chain $S_1 \rightarrow S_2 \rightarrow S_3 \rightarrow \dots \rightarrow S_n$, assume a platoon of n vehicles have merged on to the two-lane roundabout from the left entry lane, with $n \geq 3$, then if a new vehicle (i.e., the $(n+1)^{th}$ vehicle in the queue) can also merge into the two-lane roundabout without a full-stop, the required headways for outer circulating lane is $t_r + \frac{v_{e,0}^O}{a} + t_r + \frac{v_c^O}{a} + n * t_r + \sum_{i=1}^n \frac{v_{e,i}^O}{a} = (n+2) * t_r + \frac{v_c^O}{a} + \sum_{i=1}^n \frac{v_{e,i}^O}{a}$; the required headways for inner circulating lane is $t_r + \frac{v_{e,0}^I}{a} + t_r + \frac{v_e^I}{a} + n * t_r + \sum_{i=1}^n \frac{v_{e,i}^I}{a} = (n+2) * t_r + \frac{(n+1)*v_c^O}{a} + \frac{v_e^I}{a}$. Hence,

$$\int_{(n+2)*t_r + \frac{v_c^O}{a} + \sum_{i=1}^n \frac{v_{e,i}^O}{a}}^{\infty} \lambda^O e^{-\lambda^O t} dt + \int_{(n+2)*t_r + \frac{(n+1)*v_c^O}{a} + \frac{v_e^I}{a}}^{\infty} \lambda^I e^{-\lambda^I t} dt = e^{-\lambda^O * \left(t_r + \frac{v_{e,n}^O}{a}\right) - \lambda^I * \left(t_r + \frac{v_c^O}{a}\right)},$$

$$\int_{(n+1)*t_r + \frac{v_c^O}{a} + \sum_{i=1}^{n-1} \frac{v_{e,i}^O}{a}}^{\infty} \lambda^O e^{-\lambda^O t} dt + \int_{(n+1)*t_r + \frac{n*v_c^O}{a} + \frac{v_e^I}{a}}^{\infty} \lambda^I e^{-\lambda^I t} dt$$

$$P^L(S_1/S_3) = 1 - P^L(S_1/S_2) = 1 - e^{-\lambda^O * \left(t_r + \frac{v_{e,n}^O}{a}\right) - \lambda^I * \left(t_r + \frac{v_c^O}{a}\right)}, \text{ in which } v_{e,n}^O \leq v_c^O \text{ and we have } P^L(S_2/S_3) = 0.$$

Similar as the single lane scenario, we then enumerate four different categories of state transition chain.

Entry vehicle pattern 1: no vehicle can enter the two-lane roundabout from left entry lane in an episode, the probability is $P^L(S_1 \rightarrow S_1) = P^L(S_1) * P^L(S_1/S_1) = 1 - e^{-\lambda^O * \left(2t_r + \frac{v_c^O}{a}\right) - \lambda^I * \left(2t_r + \frac{v_c^O + v_e^I}{a}\right)}$.

Entry vehicle pattern 2: exactly one vehicle can enter the two-lane roundabout from left entry lane in an episode. The corresponding state transition

$$P^L(S_1 \rightarrow S_2 \rightarrow S_1) = P^L(S_1 \rightarrow S_2) *$$

chain is $S_1 \rightarrow S_2 \rightarrow S_1$. The probability is

$$P^L(S_2 \rightarrow S_1) = P^L(S_2/S_1) * P^L(S_1/S_2) = e^{-\lambda^O * \left(2t_r + \frac{v_c^O}{a}\right) - \lambda^I * \left(2t_r + \frac{v_c^O + v_e^I}{a}\right)} - e^{-\lambda^O * \left(3t_r + \frac{v_c^O + v_{e,1}^O}{a}\right) - \lambda^I * \left(3t_r + \frac{2v_c^O + v_e^I}{a}\right)}.$$

Entry vehicle pattern 3: exactly two vehicles can enter the two-lane roundabout from left entry lane in an episode. The corresponding state

$$P^L(S_1 \rightarrow S_2 \rightarrow S_3 \rightarrow S_1) = P^L(S_1 \rightarrow S_2) * P^L(S_2 \rightarrow S_3) * P^L(S_3 \rightarrow S_1) =$$

transition chain is $S_1 \rightarrow S_2 \rightarrow S_3 \rightarrow S_1$. The probability is

$$e^{-\lambda^O * \left(3*t_r + \frac{v_c^O + v_{e,1}^O}{a}\right) - \lambda^I * \left(3*t_r + \frac{2v_c^O + v_e^I}{a}\right)} - e^{-\lambda^O * \left(4*t_r + \frac{v_c^O + v_{e,1}^O + v_{e,2}^I}{a}\right) - \lambda^I * \left(4*t_r + \frac{3v_c^O + v_e^I}{a}\right)}.$$

Entry vehicle pattern 4: more than two vehicles can enter the two-lane roundabout from left entry lane in an episode. When n vehicles can merge into the two-lane roundabout from left entry lane, with $n > 2$, the corresponding state transition chain is $S_1 \rightarrow S_2 \rightarrow S_3 \rightarrow \dots \rightarrow S_n \rightarrow S_1$. The probability of this state transition chain is derived in Eq. (19). For detailed derivation, please refer to Appendix-B.

$$P^L(S_1 \rightarrow S_2 \rightarrow S_3 \rightarrow \dots \rightarrow S_n \rightarrow S_1) = P^L(S_1 \rightarrow S_2) * P^L(S_2 \rightarrow S_3) * P^L(S_3 \rightarrow S_4) * \dots * P^L(S_n \rightarrow S_1) = \\ e^{-\lambda^O * \left((n+1)*t_r + \frac{v_c^O + \sum_{i=1}^{n-1} v_{e,i}^O}{a}\right) - \lambda^I * \left((n+1)*t_r + \frac{n*v_c^O + v_e^I}{a}\right)} - e^{-\lambda^O * \left((n+2)*t_r + \frac{v_c^O + \sum_{i=1}^n v_{e,i}^O}{a}\right) - \lambda^I * \left((n+2)*t_r + \frac{(n+1)*v_c^O + v_e^I}{a}\right)} \quad (19)$$

$$N^L(T, Q_c^O, Q_c^I, v_c^O, v_e^I, v_e^O) = T * \min(Q_c^O, Q_c^I) *$$

Similarly, $\sum_{n=1}^{\infty} n * \left(e^{-\lambda^O * \left((n+1)*t_r + \frac{v_c^O + \sum_{i=1}^{n-1} v_{e,i}^O}{a}\right) - \lambda^I * \left((n+1)*t_r + \frac{n*v_c^O + v_e^I}{a}\right)} - e^{-\lambda^O * \left((n+2)*t_r + \frac{v_c^O + \sum_{i=1}^n v_{e,i}^O}{a}\right) - \lambda^I * \left((n+2)*t_r + \frac{(n+1)*v_c^O + v_e^I}{a}\right)}\right)$. We have and

$$N^L(T, Q_c^O, Q_c^I, v_c^O, v_e^I, v_e^O) = T * \min(Q_c^O, Q_c^I) * [e^{-\lambda^O * \left(2*t_r + \frac{v_c^O}{a}\right) - \lambda^I * \left(2*t_r + \frac{v_c^O + v_e^I}{a}\right)} + e^{-\lambda^O * \left(3*t_r + \frac{v_c^O}{a}\right) - \lambda^I * \left(3*t_r + \frac{2v_c^O + v_e^I}{a}\right)}]$$

$$e^{-\lambda^O * \left(4*t_r + \frac{8*v_c^O}{a}\right) - \lambda^I * \left(4*t_r + \frac{3*v_c^O + v_e^I}{a}\right)} + e^{-\lambda^O * \left(5*t_r + \frac{11*v_c^O}{a}\right) - \lambda^I * \left(5*t_r + \frac{4*v_c^O + v_e^I}{a}\right)} + e^{-\lambda^O * \left(6*t_r + \frac{15*v_c^O}{a}\right) - \lambda^I * \left(6*t_r + \frac{3*v_c^O + v_e^I}{a}\right)} - 5e^{-\lambda^O * \left(7*t_r + \frac{19*v_c^O}{a}\right) - \lambda^I * \left(7*t_r + \frac{4*v_c^O + v_e^I}{a}\right)}$$

detailed derivation, please refer to Appendix B.

$$N^L(T, Q_c^O, Q_c^I, v_c^O, v_c^I, v_e^O) = T * \min(Q_c^O, Q_c^I) * [e^{-\lambda^O * \left(2 * t_r + \frac{v_c^O}{a}\right)} - \lambda^I * \left(2 * t_r + \frac{v_c^O + v_c^I}{a}\right)] + \\ e^{-\lambda^O * \left(3 * t_r + \frac{\frac{6}{5}v_c^O}{a}\right)} - \lambda^I * \left(3 * t_r + \frac{2 * v_c^O + v_c^I}{a}\right) + e^{-\lambda^O * \left(4 * t_r + \frac{\frac{8}{5}v_c^O}{a}\right)} - \lambda^I * \left(4 * t_r + \frac{3 * v_c^O + v_c^I}{a}\right) + e^{-\lambda^O * \left(5 * t_r + \frac{11}{5}v_c^O\right)} - \lambda^I * \left(5 * t_r + \frac{4 * v_c^O + v_c^I}{a}\right)$$

Plug in N_1^L and N_2^L , we can get $e^{-\lambda^O * \left(6 * t_r + \frac{3 * v_c^O}{a}\right)} - \lambda^I * \left(6 * t_r + \frac{5 * v_c^O + v_c^I}{a}\right) + \lim_{N \rightarrow \infty} \sum_{i=5}^{N-1} e^{-\lambda^O * \left((i+2) * t_r + \frac{(i-1) * v_c^O}{a}\right)} - \lambda^I * \left((i+2) * t_r + \frac{(i+1) * v_c^O + v_c^I}{a}\right)$. Since

$$\lim_{N \rightarrow \infty} N e^{-\lambda^O * \left((N+2) * t_r + \frac{(N-1) * v_c^O}{a}\right)} - \lambda^I * \left((N+2) * t_r + \frac{(N+1) * v_c^O + v_c^I}{a}\right)]$$

$\lim_{N \rightarrow \infty} \sum_{i=5}^{N-1} e^{-\lambda^O * \left((i+2) * t_r + \frac{(i-1) * v_c^O}{a}\right)} - \lambda^I * \left((i+2) * t_r + \frac{(i+1) * v_c^O + v_c^I}{a}\right)$ is a geometric sequence, its summation is

$$\lim_{N \rightarrow \infty} \sum_{i=5}^{N-1} e^{-\lambda^O * \left((i+2) * t_r + \frac{(i-1) * v_c^O}{a}\right)} - \lambda^I * \left((i+2) * t_r + \frac{(i+1) * v_c^O + v_c^I}{a}\right) = \frac{e^{-\lambda^O * \left(7 * t_r + \frac{4 * v_c^O}{a}\right)} - \lambda^I * \left(7 * t_r + \frac{6 * v_c^O + v_c^I}{a}\right)}{1 - e^{-\lambda^O * \left(t_r + \frac{v_c^O}{a}\right)} - \lambda^I * \left(t_r + \frac{v_c^O}{a}\right)}$$

$$\lim_{N \rightarrow \infty} N e^{-\lambda^O * \left((N+2) * t_r + \frac{(N-1) * v_c^O}{a}\right)} - \lambda^I * \left((N+2) * t_r + \frac{(N+1) * v_c^O + v_c^I}{a}\right) = \lim_{N \rightarrow \infty} \frac{N}{e^{-\lambda^O * \left((N+2) * t_r + \frac{(N-1) * v_c^O}{a}\right)} - \lambda^I * \left((N+2) * t_r + \frac{(N+1) * v_c^O + v_c^I}{a}\right)} = 0. \text{ For a detailed derivation, please refer}$$

to Appendix B. Also, as $\lambda^O = Q_c^O / 3600$, $\lambda^I = Q_c^I / 3600$, and $Q_e^L = \frac{N^L(T, Q_c^O, Q_c^I, v_c^O, v_c^I, v_e^O)}{T}$, we can further reformulate to compute the roundabout left entry lane capacity $Q_e^L = \min(Q_c^O, Q_c^I) * [e^{-\frac{Q_e^O}{3600} * \left(2 * t_r + \frac{v_c^O}{a}\right)} - \frac{Q_e^I}{3600} * \left(2 * t_r + \frac{v_c^O + v_c^I}{a}\right) + e^{-\frac{Q_e^O}{3600} * \left(3 * t_r + \frac{6 * v_c^O}{a}\right)} - \frac{Q_e^I}{3600} * \left(3 * t_r + \frac{2 * v_c^O + v_c^I}{a}\right) + e^{-\frac{Q_e^O}{3600} * \left(4 * t_r + \frac{\frac{6}{5}v_c^O}{a}\right)} - \frac{Q_e^I}{3600} * \left(4 * t_r + \frac{3 * v_c^O + v_c^I}{a}\right) + e^{-\frac{Q_e^O}{3600} * \left(5 * t_r + \frac{11}{5}v_c^O\right)} - \frac{Q_e^I}{3600} * \left(5 * t_r + \frac{4 * v_c^O + v_c^I}{a}\right) + e^{-\frac{Q_e^O}{3600} * \left(6 * t_r + \frac{16}{5}v_c^O\right)} - \frac{Q_e^I}{3600} * \left(6 * t_r + \frac{5 * v_c^O + v_c^I}{a}\right) + e^{-\frac{Q_e^O}{3600} * \left(7 * t_r + \frac{21}{5}v_c^O\right)} - \frac{Q_e^I}{3600} * \left(7 * t_r + \frac{6 * v_c^O + v_c^I}{a}\right)]$.

If we use $\tau_i^{L,O}$ and $\tau_i^{L,I}$ to denote the required headway gap in the outer and inner circulating flow for a total of i entry vehicles to safely merge into the roundabout from left entry lane, the roundabout left-lane capacity Q_e^L becomes:

$$Q_e^L = \min(Q_c^O, Q_c^I) * \left(\sum_{i=1}^5 e^{-\frac{Q_e^O}{3600} * \tau_i^{L,O}} - \frac{Q_e^I}{3600} * \tau_i^{L,I} + \frac{e^{-\frac{Q_e^O}{3600} * \tau_6^{L,O}} - \frac{Q_e^I}{3600} * \tau_6^{L,I}}{1 - e^{-\frac{Q_e^O}{3600} * \left(t_r + \frac{v_c^O}{a}\right)} - \frac{Q_e^I}{3600} * \left(t_r + \frac{v_c^O}{a}\right)} \right) \quad (20)$$



(a) Roundabout 1



(b) Roundabout 2



(c) Roundabout 3



(d) Roundabout 4

Fig. 6. Overview of the four roundabouts in openDD dataset

In which $\tau_1^{L,O} = 2 * t_r + \frac{v_c^O}{a}$, $\tau_1^{L,I} = 2 * t_r + \frac{v_c^O + v_c^I}{a}$, $\tau_2^{L,O} = 3 * t_r + \frac{\frac{6}{5}v_c^O}{a}$, $\tau_2^{L,I} = 3 * t_r + \frac{2*v_c^O + v_c^I}{a}$, $\tau_3^{L,O} = 4 * t_r + \frac{\frac{8}{5}v_c^O}{a}$, $\tau_3^{L,I} = 4 * t_r + \frac{3*v_c^O + v_c^I}{a}$, $\tau_4^{L,O} = 5 * t_r + \frac{\frac{11}{5}v_c^O}{a}$, $\tau_4^{L,I} = 5 * t_r + \frac{4*v_c^O + v_c^I}{a}$, $\tau_5^{L,O} = 6 * t_r + \frac{3*v_c^O}{a}$, $\tau_5^{L,I} = 6 * t_r + \frac{5*v_c^O + v_c^I}{a}$, $\tau_6^{L,O} = 7 * t_r + \frac{4*v_c^O}{a}$ and $\tau_6^{L,I} = 7 * t_r + \frac{6*v_c^O + v_c^I}{a}$.

5. Numerical analysis

In this section, a case study is conducted with a real-world dataset. An overview of the dataset is presented first. We then analyze the accuracy of the proposed model and compare it with the HCM6 model. Finally, a sensitivity analysis is performed.

5.1. Data description

OpenDD, a large-scale roundabout drone dataset at four roundabouts, is utilized in this section (Breuer et al., 2020). The alignments of the roundabouts are given in Fig. 6 below. The drone camera is capturing vehicle trajectories, at a speed of 30 frames per second (fps), which is equivalent to a time interval of 0.03 s. All four selected roundabouts could be considered as regular ones with four legs and a single circulating lane. Hence, they could be viewed as general scenarios to test the performance of the proposed model.

In the dataset, each row contains information on a trajectory point of a given object, e.g., passenger car, van, or truck, at a given snapshot with a total of 14 columns/attributes. Table 2 below shows sample data from the dataset, in which only the most critical and relevant information is displayed. Starting from left, each column denotes the time, ID, x-part and y-part of the UTM 32N coordinate, bounding box angle relative to the UTM 32N x-axis, velocity, acceleration and class of the given object instance. To summarize, two main categories of information are provided, including the relative location to the roundabout, and the movement status of entering vehicles. Based on this information, the circulating flow in the roundabout and the congestion degree at each entrance can be inferred, which could help to derive the entering capacity of the roundabout.

Table 3 below presents some statistical characteristics of the dataset. Each roundabout contains at least 7 hr of recording, with at least 2 h during rush period in the morning and afternoon, as well as regular time in between rush hours. Therefore, different degrees of congestion at each roundabout leg are captured with a sufficient length of recording. Thousands of passenger cars are captured in each roundabout. For each vehicle, the complete movement trajectory is recorded, including merging, circulating, and diverging behaviors.

We process the data in the following manner. According to the definition of roundabout entry capacity, the time periods in which at least one vehicle is always queued at the give-way line of the entry lane is first identified, and we then extract such video recordings from the dataset. Driver response time t_r is set to be 1.33 s, on average (Henry and Sabra 2005), and the vehicle max deceleration value a is set as 4.51 m/s^2 or 14.8 ft/s^2 (Fambro et al., 1997). Besides, circulating flow speed v_c ranges from 23.78 km/h to 26.10 km/h for the four roundabouts. The duration of the analysis period, i.e., the length of the video clips to extract, is set as 30 s, so that it won't be too long to include under-saturated traffic flow, or too short to include sharp fluctuations in results.

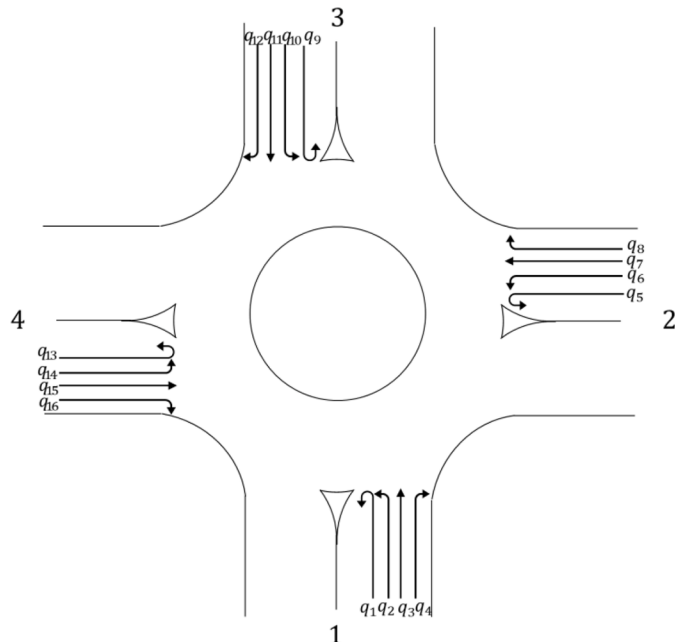


Fig. 7. Traffic flow movements in a roundabout (q_i denotes the traffic flow of turning movements).

Table 2
Sample trajectory data.

ID	TIMESTAMP	OBJID	UTM_X	UTM_Y	UTM_ANGLE	V	ACC	CLASS
1	0	76637	673963.4	5410643	2.763985307	7.89	1.1214	Car
2	0.033367	76637	673963.2	5410643	2.775185307	7.89	1.2746	Car
3	0.066733	76637	673962.9	5410643	2.784785307	7.89	1.4303	Car

Table 3
Statistics of the openDD dataset, distinguishing the four included roundabouts.

Data Subset	Roundabout 1	Roundabout 2	Roundabout 3	Roundabout 4
Recorded time	7.0 h	7.7 h	7.7 h	7.5 h
# drone flights	54	69	57	56
# passenger car trajectories	7,100	5,983	6,512	7,685
Average # records of passenger car	385	477	423	481
Average trajectory duration of passenger car	12.69 s	15.74 s	13.96 s	16.01 s
Average trajectory length of passenger car	80.76 m	111.55 m	108.27 m	120.77 m

5.2. Accuracy analysis

For each video recording, two benchmark models are utilized for comparison. The first is HCM6 model with its prediction results denoted by Q_e^h (h for HCM). The second is a new gap-acceptance based model (NGA model) by incorporating the effects of the exiting vehicles proposed by Qu et al. (2014). The formula is $Q_e^n = Q_c' * \left[\rho + \frac{\exp(-Q'_c * \frac{t_f}{3600})}{1 - \exp(-Q'_c * \frac{t_f}{3600})} \right]$, where Q_e^n is entry capacity (n for new gap-acceptance), Q'_c is new conflicting circulating flow with existing vehicles at the saturated leg are included; ρ is the proportion of these exiting vehicles out of circulating flow. To calculate the conflicting circulating flow, for the proposed model, we adopted the same approach as HCM6 (TRB, 2016) which sums up the conflicting turning traffic from various approaches to get the circulating flow. As Fig. 8 shows, in a single lane roundabout, each entry leg has four turning movements, right turn, straight, left turn and U-turn, with q_i denoting the respective traffic flow. Take Approach 1 as an example, the circulating flow $Q_{c,1}$ is $q_5 + q_9 + q_{10} + q_{13} + q_{14} + q_{15}$, which is comprised of the U-turn flow of Approach 2; the left turn and U-turn flow of Approach 3; the straight, left turn and U-turn flow of Approach 4. Correspondingly, the new circulating flow Q'_c for NGA can be calculated by adding the existing traffic flow at the queueing leg. For the same example, the new circulating flow at Approach 1 $Q'_{c,1}$ equals $Q_{c,1} + q_1 + q_6 + q_{11} + q_{16}$, which adds the left turn flow of Approach 2, the straight flow of Approach 3 and the right turn flow of Approach 4 to the circulating flow $Q_{c,1}$. In addition, for the NGA model, the proportion of the exiting vehicles out of circulating flow at Approach 1 ρ_1 equals $1 - \frac{Q_{c,1}}{Q'_{c,1}}$.

For the HCM6 model and the NGA model, we calibrated the critical gap t_c and follow-up headway t_f of for the four roundabouts. Follow-up headway was calibrated by taking the average of headway observation between two consecutively entering vehicles, utilizing the same gap in the circulating follow, which ranges from 2.51 s to 3.10 s in this case. Critical headway was calculated by maximum likelihood method (Troutbeck, 2014). It is assumed that a driver's critical gap is between the largest rejected gap and the

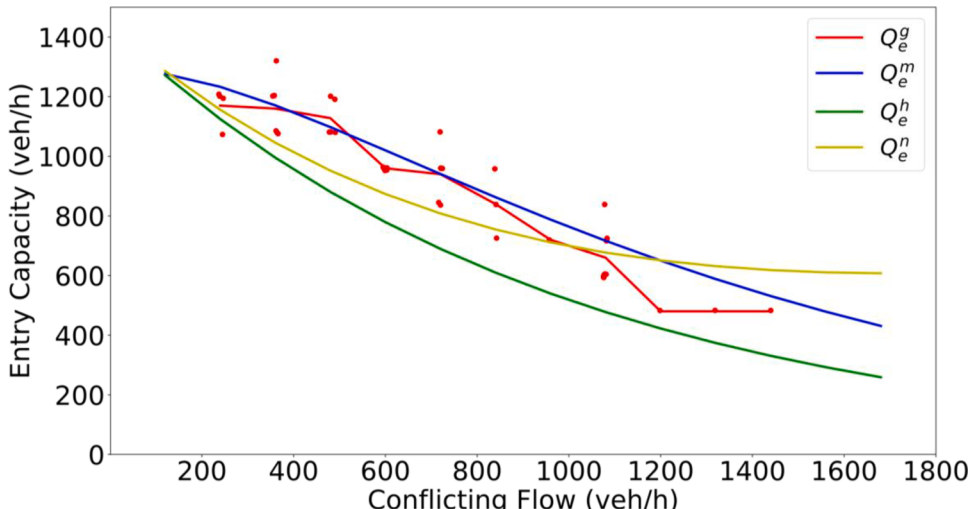


Fig. 8. Entry capacity calculation results for Roundabout #1 (Q_e^m for proposed model, Q_e^h for HCM, Q_e^n for NGA, and Q_e^g for ground truth).

smallest accepted gap, and that the distribution of critical gaps is lognormal. By maximizing the logarithm of the likelihood $L = \sum_{i=1}^n \ln[F(a_i) - F(r_i)]$, where a_i is gap accepted by the i th driver; r_i is the largest gap rejected by the i th driver (equal to 0 if no gap was rejected); $F(x)$ is the cumulative distribution function of critical gaps. In this case, critical gap ranges from 4.59 s to 5.40 s for the four roundabouts.

We use Q_e^m to denote model prediction results (m for the proposed model) and Q_e^g to denote ground truth capacity (g for ground truth) and, for each video recording, we compare Q_e^m , Q_e^n , Q_e^h , and Q_e^g , which are all in pc/h. Since each roundabout leg may have several video recordings that qualify as saturation traffic flow, we aggregate errors of the multiple observations for the same roundabout leg. We use mean absolute percentage error (MAPE) to evaluate the prediction accuracy. $MAPE_e^m = \frac{1}{num} \sum_{i=1}^{num} abs\left(\frac{Q_{ei}^g - Q_{ei}^m}{Q_{ei}^g}\right)$, $MAPE_e^h = \frac{1}{num} \sum_{i=1}^{num} abs\left(\frac{Q_{ei}^g - Q_{ei}^h}{Q_{ei}^g}\right)$, in which num is the number of video recordings that traffic is saturated at the target roundabout leg. Certainly, lower MAPE values are preferred.

We first visualize the detailed comparison results of roundabout 1 in Fig. 8 below. The green curve represents results from the HCM6 model, with a calibrated critical headway of 4.90 s, and a follow-up headway of 2.51 s. The shape of this curve is identical to those from the literature (Robinson et al., 2010; Yap et al., 2013). The red curve is the ground truth data straight from an open DD dataset, and the blue curve is the results from the proposed model. The β value is found to be 1.03 for this roundabout, and the circulation speed is 6.60m/s, or 23.77 km/h. It can be found that the overall, HCM model is underestimating roundabout capacity, which is consistent with what is reported in the literature (Chen and Hourdos 2018). The prediction capacity of NGA model is higher than HCM model, which is consistent with the evaluation by Ren et al. (2016). On the other hand, the proposed model is able to generate results that are more aligned with ground truth data, with some overestimation and some underestimation observed. The results show the mean absolute percentage error of the HCM6 and NGA model are 21.03% and 13.53%, whereas the mean absolute percentage error of the proposed model is 9.52%, marking a significant improvement.

Table 4 below lists the detailed results of comparisons of all roundabouts and all approaches from the openDD dataset. Besides a mean absolute percentage error, we also show the number of qualified datasets for each roundabout approach, i.e., the number of video clips that have at least one vehicle always waiting at the give-way line of the entry lane during each 30-s analysis period. It can be observed that, except for the western leg of roundabout 1, as well as the eastern and northern legs of roundabout 2, the drones are always able to capture saturated traffic flow conditions for multiple times at each roundabout leg. Most roundabout legs have over 5 valid datasets, which means the data size should be sufficient to draw statistically significant conclusions. When comparing the accuracy of the proposed model and the HCM and the NGA model, it is found that the proposed model is able to consistently achieve a lower MAPE than the HCM and the NGA model. The $MAPE_e^h$ and $MAPE_e^m$ of all roundabout approaches range from 14% to 32% and from 10% to 38%, whereas $MAPE_e^n$ is in the range of 7%~17%. When all legs are combined, the MAPE value drops from 21.03% and 12.36% to 9.39% for the first roundabout, from 26.38% and 19.67% to 15.55% for the second roundabout, from 17.73% and 16.17% to 9.84% for the third roundabout, and from 24.72% and 18.33% to 9.60% for the fourth roundabout. Experiments with 60-s analysis period were also performed, and the proposed model was shown to consistently outperform the two benchmark models. However, the number of qualified datasets was further decreased, and the results are not shown here.

Table 4
Entry capacity calculation results of each entrance of four roundabouts.

Approach	Measurement	Roundabout 1	Roundabout 2	Roundabout 3	Roundabout 4
Northern Leg	Number of qualified datasets	15	0	1	2
	$MAPE_e^m$ (this model)	11.09%	N/A	13.60%	5.12%
	$MAPE_e^h$ (HCM6 approach)	18.76%	N/A	15.28%	32.38%
	$MAPE_e^n$ (NGA model)	15.29%	N/A	16.30%	19.00%
Southern Leg	Number of qualified datasets	3	4	6	7
	$MAPE_e^m$ (this model)	13.88%	11.67%	14.53%	6.67%
	$MAPE_e^h$ (HCM6 approach)	22.73%	30.64%	24.71%	23.79%
	$MAPE_e^n$ (NGA model)	14.74%	24.68%	38.24%	17.92%
Western Leg	Number of qualified datasets	0	10	6	6
	$MAPE_e^m$ (this model)	N/A	17.11%	9.70%	11.98%
	$MAPE_e^h$ (HCM6 approach)	N/A	24.67%	14.15%	28.77%
	$MAPE_e^n$ (NGA model)	N/A	17.67%	12.77%	20.06%
Eastern Leg	Number of qualified datasets	26	0	19	10
	$MAPE_e^m$ (this model)	7.88%	N/A	8.21%	11.12%
	$MAPE_e^h$ (HCM6 approach)	22.15%	N/A	16.79%	21.42%
	$MAPE_e^n$ (NGA model)	10.39%	N/A	10.27%	17.45%
All legs combined	Number of qualified datasets	44	14	32	25
	$MAPE_e^m$ (this model)	9.39%	15.55%	9.84%	9.60%
	$MAPE_e^h$ (HCM6 approach)	21.03%	26.38%	17.73%	24.72%
	$MAPE_e^n$ (NGA model)	12.36%	19.67%	16.17%	18.33%

5.3. Sensitivity analysis

In this subsection, the sensitivity of the proposed model is examined with respect to circulating flow rate Q_c , circulating flow speed v_c , traffic circulating index β , and analysis duration length T .

We first focus on the general scenario in Section 4.1, and change Q_c and v_c , which impact the number of headway gaps in the traffic flow, as well as the acceptable headway gaps for an entry vehicle to safely merge into the roundabout. The range of Q_c is set to be [200, 1200] with a unit of vehicles/hr, and the range of v_c is set to be [15, 32.5] with a unit of km/hr. Then, the entry capacity Q_e^m is calculated under various combinations of Q_c and v_c and is shown in Fig. 9. The results show that the highest roundabout capacity is achieved when both Q_c and v_c take the lowest value, and the highest capacity is around 1,500 vehicles/hr. When Q_c is fixed, capacity decreases with an increase in v_c . This is consistent with our general understanding that, when v_c increases, to avoid a traffic crash, the required headway to safely merge into the roundabout becomes longer and, thus, Q_e^m becomes lower. On the other hand, when v_c is fixed, capacity decreases with the increase in Q_c . This is because, as a circulating vehicle rate increases, the conflicting degree between the circulating vehicle and entry vehicles also increases and, thus, the capacity drops. The lowest capacity is observed to be around 500 vehicles/hr, with given ranges of Q_c and v_c .

Next, we focus on the scenario of all four approaches being saturated. We adjust the values of β and v_c , and observe how the result changes. Fig. 10 below shows that the highest roundabout capacity is achieved when both β and v_c take the lowest value. The highest capacity is around 1,300 vehicles/hr, which is lower than the maximum capacity achieved in Fig. 9. This is understandable, as now we have all four approaches being saturated, so the lower bound of circulating traffic flow rate is higher than that used in Fig. 9. When β is fixed, Q_e^m decreases with an increase in v_c . On the other hand, when v_c is fixed, Q_e^m decreases with the increase in β . The physical implication is, if circulating vehicles travel for longer distances in the roundabout before taking an exit, the vehicle demand in the roundabout becomes higher with smaller headway gaps. Therefore, the entry capacity of a roundabout is reduced, due to the denser circulating stream flow. The lowest capacity is also observed to be around 500 vehicles/hr, with given ranges of β and v_c .

We also examine the impact of an analysis duration on the modeling results. As discussed earlier, we only extract the subset of a drone dataset when at least one vehicle is waiting at the give-way line of the entry lane, so that the extracted dataset can be said to qualify for saturation traffic. We assume that the vehicle headway is subject to negative exponential distribution. However, in reality, a vehicle's arrival may be more random, or subject to other constraints, such as upstream intersections or pedestrians. If the duration of observation is set for too long, it could be challenging to find a period of time that the roundabout is consistently saturated throughout the analysis period. On the other hand, if the duration of observation is too short (for example, less than 10 s), the number of vehicles that can merge into the roundabout could be very low, and a small change in this number could lead to a sharp fluctuation in the final results. As such, the range of analysis duration is set as [10, 60] with a unit of a second. In Fig. 11, the MAPEs of the HCM model, NGA model and the proposed model under different analysis durations, are shown.

As observed in Fig. 11, it is obvious that, when compared with the HCM model (marked in blue color) and NGA model (marked in yellow color), the MAPE of the proposed model (red line) is always lower, no matter what time duration is used. This pattern is consistently observed for all four roundabouts. The proposed model achieves the best performance when the analysis duration is set as 30 s, whereas if the duration is too short or too long, the modeling performances drops although, in general, it remains in a range of 10–20%. For the HCM6 model, a consistent trend is noticed that, when the analysis duration increases, the MAPE drops. One possible

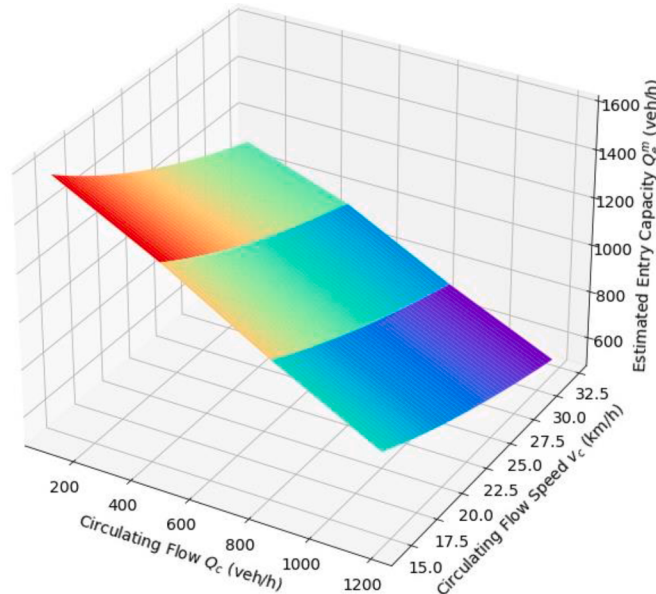


Fig. 9. Entry capacity Q_e^m under various Q_c and v_c .

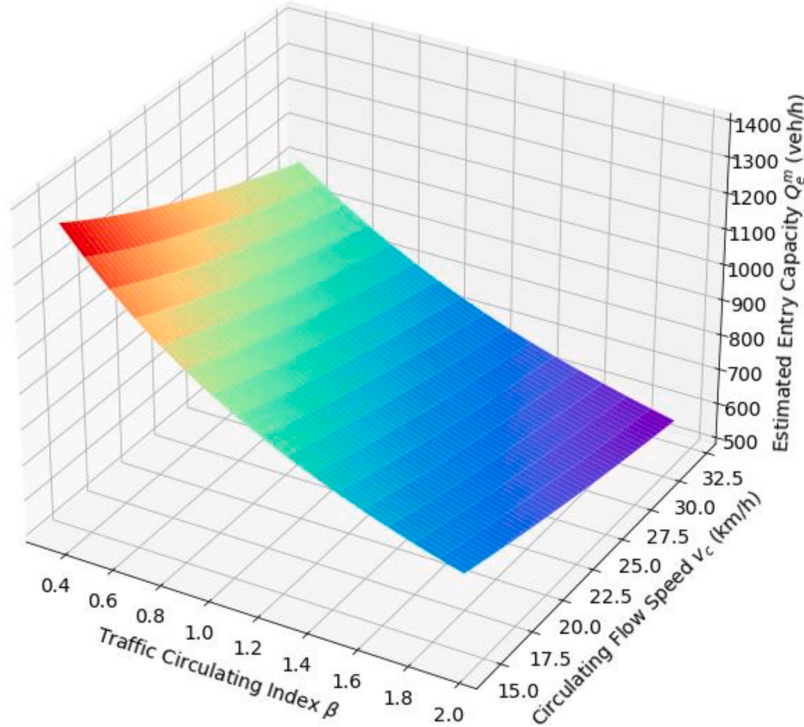


Fig. 10. Entry capacity Q_e^m under various β and v_c .

explanation is that the HCM6 model is underestimating the capacity (as shown in Fig. 8 and suggested by (Chen and Hourdos 2018)). So, when the analysis duration is set to be longer, the roundabout approach may include under-saturated flow during the analysis period and, thus, the ground truth capacity will drop, which makes a difference with underestimated HCM6 smaller results.

6. Conclusions

In this manuscript, modeling efforts are made to advance the causality and theoretical understanding of roundabout capacity inference. A merging state transition-based analytical approximation and calibration approach is presented, with circulating speed, driver perception response time, and vehicle maximum deceleration as the key inputs. We note that the usage of circulating speed in the proposed model can, not only serve a similar purpose as a critical gap in gap-acceptance model, but it is also able to reflect the operation condition factors that are specifically related to a roundabout of interest. Calibration of circulating speed is also relatively easy with existing data sources; for example, with the partial vehicle trajectory data from a smartphone or connected vehicles.

A case study is conducted with OpenDD, a real-world high-resolution trajectory dataset collected by drones, with a time interval of 0.03 s, at four standard roundabouts. Each roundabout has at least 7 h of recording, with at least 2 h during the rush period in the morning and afternoon, as well as the regular time between rush hours. It is found that the proposed model is able to consistently achieve a lower MAPE than the HCM and the NAG model. The $MAPE_e^h$ and $MAPE_e^n$ of all roundabout approaches range from 14% to 32% and from 10% to 38%, whereas $MAPE_e^m$ is in the range of 7–17%. The sensitivity of the proposed model is also examined with respect to circulating flow rate Q_c , circulating flow speed v_c , traffic circulating index β , and analysis duration length T . It is found that the capacity decreases with the increase in Q_c , v_c , and β . The proposed model achieves the best performance when the analysis duration T is set as 30 seconds, whereas, when the duration is too short or too long, the modeling performance drops, but still remains in a range of 10–20%, and consistently outperforms the two benchmark models.

Future research may be focused on multi-lane roundabouts, where a new coefficient may be introduced to reflect more complex merging behavior, although we envision the modeling framework and the analytical derivation shown in this manuscript will still be applicable. In addition, since the utilized dataset only includes data from the standard roundabout, the model's performance for a non-standard roundabout, such as compact roundabout and turbo roundabout, can be further investigated.

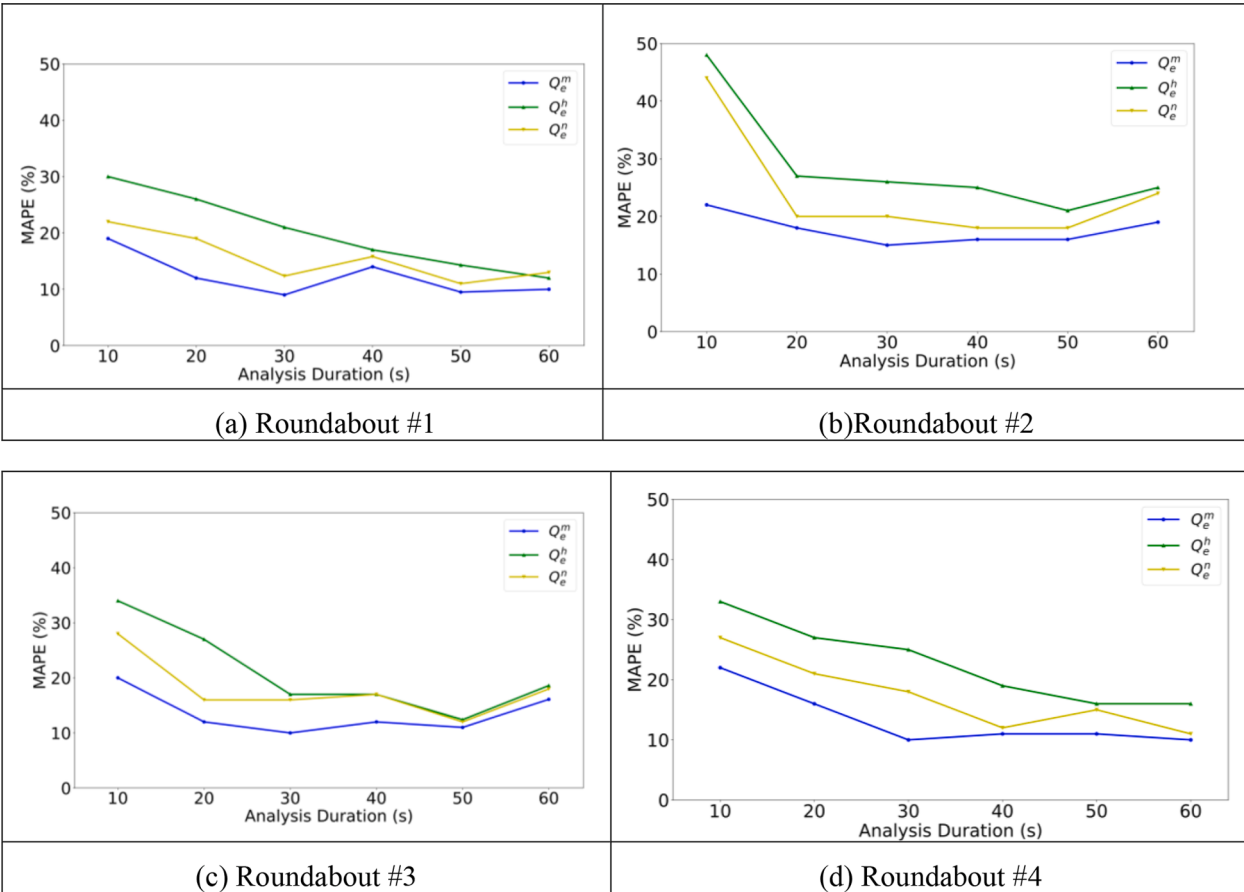


Fig. 11. Estimation results under different analysis periods.

CRediT authorship contribution statement

Yang Song: Formal analysis, Validation, Visualization, Writing – original draft. **Xianbiao Hu:** Conceptualization, Methodology, Supervision, Writing – original draft. **Jiawei Lu:** Validation, Visualization. **Xuesong Zhou:** Conceptualization, Methodology, Writing – original draft.

Appendices. Appendix A – Notation List

t_c :	Critical gap
$t_{c,lead}$:	A minimum time headway with the leading circulating vehicle that could allow merging
$t_{c,lag}$:	A minimum time headway with the lagging circulating vehicle that could allow merging
t_f :	Follow-up headway
t_r :	Driver response time
τ_i :	headway gap for a total of i entry vehicles to safely merge into the roundabout
Q_c :	Circulating flow rate (veh/h)
λ :	Circulating flow, equivalent to $Q_c/3600$
Q_e :	Entry capacity (veh/h)
v_c :	Circulating flow speed (km/h)
v_e :	Entry flow speed (km/h)
$v_{e,i}$:	Approaching speed of the i th vehicle arriving at roundabout stop line (km/h)
β :	Traffic circulating index
a :	Vehicle max deceleration value (m/s^2)
A, B :	Two parameters of HCM6 model
l_e :	Number of entry lanes
l_c :	Number of circulating lanes
Δ :	Intra-bunch minimum headway within each bunch in the circulating flow (s)
λ :	A scale parameter or decay rate
h :	Time headway in the roundabout traffic flow
T :	Defined time duration for capacity analysis
$N(Q_c, v_c)$:	Number of vehicles that can enter roundabout within time T
p_i :	The probability that a vehicle gets off at next i th exit, $i \in \{1, 2, 3, 4\}$
$f(v_c, \beta; t_r, a)$:	Auxiliary function with Q_c as dependent variable
$g(Q_c)$:	Auxiliary function with Q_c as independent variable
n_c :	Number of circulating vehicles
n_e :	Number of entry vehicles entering from the saturated entrance
$n_{e,i}$:	Number of entry vehicles entering from the saturated entrance, leaving at the next i th exit, $i \in \{1, 2, 3, 4\}$
Q_c^m :	Circulating flow derived by the proposed model
Q_e^m :	Entry capacity derived by the proposed model
Q_e^h :	Entry capacity derived by HCM6 model
Q_c^g :	Ground-truth value of circulating flow
Q_e^g :	Ground-truth value of entry capacity
$RMSE_e^m$:	Root mean square error of the proposed model
$RMSE_e^h$:	Root mean square error of HCM6 model
num_{sat} :	Number of saturated time durations for an entrance

Appendix B – Some Derivations

B.1. Derivation of $P(S_1 \rightarrow S_2 \rightarrow S_3 \rightarrow \dots \rightarrow S_n \rightarrow S_1)$ in Eq. (7)

$$\begin{aligned}
 P(S_1 \rightarrow S_2 \rightarrow S_3 \rightarrow \dots \rightarrow S_n \rightarrow S_1) &= P(S_1 \rightarrow S_2) * P(S_2 \rightarrow S_3) * P(S_3 \rightarrow S_4) * \dots * P(S_{n-1} \rightarrow S_n) * P(S_n \rightarrow S_1) \\
 &= e^{-\lambda * \left(2t_r + \frac{v_c}{a} \right)} * e^{-\lambda * \left(t_r + \frac{v_{e,1}}{a} \right)} * e^{-\lambda * \left((n-2)t_r + \frac{\sum_{i=2}^{n-1} v_{e,i}}{a} \right)} * \left(1 - e^{-\lambda * \left(t_r + \frac{v_{e,n}}{a} \right)} \right) \\
 &\quad e^{-\lambda * \left((n+1)*t_r + \frac{v_c + \sum_{j=1}^{n-1} v_{e,j}}{a} \right)} - e^{-\lambda * \left((n+2)*t_r + \frac{v_c + \sum_{j=1}^n v_{e,j}}{a} \right)}
 \end{aligned}$$

B.2. Derivation of $N_1(T, Q_c, v_c, v_e)$ in Eq. (11).

$$\begin{aligned}
N_1(T, Q_c, v_c, v_e) &= T * Q_c * \sum_{n=1}^5 n * \left(e^{-\lambda * \left((n+1)*t_r + \frac{v_c + \sum_{i=1}^{n-1} v_{e,i}}{a} \right)} - e^{-\lambda * \left((n+2)*t_r + \frac{v_c + \sum_{i=1}^n v_{e,i}}{a} \right)} \right) \\
&= T * Q_c \left[1 * \left(e^{-\lambda * \left((1+1)*t_r + \frac{v_c + \sum_{i=1}^{1-1} v_{e,i}}{a} \right)} - e^{-\lambda * \left((1+2)*t_r + \frac{v_c + \sum_{i=1}^1 v_{e,i}}{a} \right)} \right) + 2 \right. \\
&\quad \left. * \left(e^{-\lambda * \left((2+1)*t_r + \frac{v_c + \sum_{i=1}^{2-1} v_{e,i}}{a} \right)} - e^{-\lambda * \left((2+2)*t_r + \frac{v_c + \sum_{i=1}^2 v_{e,i}}{a} \right)} \right) + 3 \right. \\
&\quad \left. * \left(e^{-\lambda * \left((3+1)*t_r + \frac{v_c + \sum_{i=1}^{3-1} v_{e,i}}{a} \right)} - e^{-\lambda * \left((3+2)*t_r + \frac{v_c + \sum_{i=1}^3 v_{e,i}}{a} \right)} \right) + 4 \right. \\
&\quad \left. * \left(e^{-\lambda * \left((4+1)*t_r + \frac{v_c + \sum_{i=1}^{4-1} v_{e,i}}{a} \right)} - e^{-\lambda * \left((4+2)*t_r + \frac{v_c + \sum_{i=1}^4 v_{e,i}}{a} \right)} \right) + 5 \right] \\
&= T * Q_c * \left[e^{-\lambda * \left(2*t_r + \frac{v_c}{a} \right)} + e^{-\lambda * \left(3*t_r + \frac{6*v_c}{a} \right)} + e^{-\lambda * \left(4*t_r + \frac{8*v_c}{a} \right)} + e^{-\lambda * \left(5*t_r + \frac{11*v_c}{a} \right)} + e^{-\lambda * \left(6*t_r + \frac{13*v_c}{a} \right)} - 5e^{-\lambda * \left(7*t_r + \frac{16*v_c}{a} \right)} \right]
\end{aligned}$$

B.3 Derivation of $N_2(T, Q_c, v_c, v_e)$ in Eq. (12)

$$\begin{aligned}
N_2(T, Q_c, v_c, v_e) &= T * Q_c * \sum_{n=6}^{\infty} n * \left(e^{-\lambda * \left((n+1)*t_r + \frac{v_c + \sum_{i=1}^{n-1} v_{e,i}}{a} \right)} - e^{-\lambda * \left((n+2)*t_r + \frac{v_c + \sum_{i=1}^n v_{e,i}}{a} \right)} \right) \\
&= T * Q_c * \left[6 * \left(e^{-\lambda * \left(7*t_r + \frac{4*v_c}{a} \right)} - e^{-\lambda * \left(8*t_r + \frac{5*v_c}{a} \right)} \right) + 7 * \left(e^{-\lambda * \left(8*t_r + \frac{5*v_c}{a} \right)} - e^{-\lambda * \left(9*t_r + \frac{6*v_c}{a} \right)} \right) + 8 \right. \\
&\quad \left. * \left(e^{-\lambda * \left(9*t_r + \frac{6*v_c}{a} \right)} - e^{-\lambda * \left(10*t_r + \frac{7*v_c}{a} \right)} \right) + \dots + N * \left(e^{-\lambda * \left((N+1)*t_r + \frac{(N-2)*v_c}{a} \right)} - e^{-\lambda * \left((N+2)*t_r + \frac{(N-1)*v_c}{a} \right)} \right) \right] \\
&= T * Q_c * \left[6 * e^{-\lambda * \left(7*t_r + \frac{4*v_c}{a} \right)} + e^{-\lambda * \left(8*t_r + \frac{5*v_c}{a} \right)} + e^{-\lambda * \left(9*t_r + \frac{6*v_c}{a} \right)} + \dots + e^{-\lambda * \left((N+1)*t_r + \frac{(N-2)*v_c}{a} \right)} \right. \\
&\quad \left. - Ne^{-\lambda * \left((N+2)*t_r + \frac{(N-1)*v_c}{a} \right)} \right] \\
&= T * Q_c * \left[6 * e^{-\lambda * \left(7*t_r + \frac{4*v_c}{a} \right)} + \lim_{N \rightarrow \infty} \sum_{i=6}^{N-1} e^{-\lambda * \left((i+2)*t_r + \frac{(i-1)*v_c}{a} \right)} - \lim_{N \rightarrow \infty} Ne^{-\lambda * \left((N+2)*t_r + \frac{(N-1)*v_c}{a} \right)} \right]
\end{aligned}$$

B.4 Derivation of $\lim_{N \rightarrow \infty} \sum_{i=5}^{N-1} e^{-\lambda * \left((i+2)*t_r + \frac{(i-1)*v_c}{a} \right)}$ in Eq. (13)

$$\begin{aligned}
\lim_{N \rightarrow \infty} \sum_{i=5}^{N-1} e^{-\lambda * \left((i+2)*t_r + \frac{(i-1)*v_c}{a} \right)} &= \lim_{N \rightarrow \infty} \frac{e^{-\lambda * \left(7*t_r + \frac{4*v_c}{a} \right)} * \left(1 - e^{-N\lambda * \left(t_r + \frac{v_c}{a} \right)} \right)}{1 - e^{-\lambda * \left(t_r + \frac{v_c}{a} \right)}} = \frac{e^{-\lambda * \left(7*t_r + \frac{4*v_c}{a} \right)} * \lim_{N \rightarrow \infty} \left(1 - e^{-N\lambda * \left(t_r + \frac{v_c}{a} \right)} \right)}{1 - e^{-\lambda * \left(t_{rps} + \frac{v_c}{a} \right)}} \\
&= \frac{e^{-\lambda * \left(7*t_r + \frac{4*v_c}{a} \right)} * (1 - 0)}{1 - e^{-\lambda * \left(t_r + \frac{v_c}{a} \right)}} = \frac{e^{-\lambda * \left(7*t_r + \frac{4*v_c}{a} \right)}}{1 - e^{-\lambda * \left(t_r + \frac{v_c}{a} \right)}}
\end{aligned}$$

B.5 Derivation of $\lim_{N \rightarrow \infty} Ne^{-\lambda * \left((N+2)*t_r + \frac{(N-1)*v_c}{a} \right)}$ in Eq. (13)

$$\lim_{N \rightarrow \infty} N e^{-\lambda \left((N+2)*t_r + \frac{(N-1)v_c}{a} \right)} = \lim_{N \rightarrow \infty} \frac{N}{e^{\lambda \left((N+2)*t_r + \frac{(N-1)v_c}{a} \right)}} = \lim_{N \rightarrow \infty} \frac{1}{\lambda * (t_r + \frac{v_c}{a}) * e^{\lambda \left((N+2)*t_r + \frac{(N-1)v_c}{a} \right)}} = 0$$

B.6 Derivation of $g'(Q_e)$

$$\begin{aligned} g'(Q_e) &= \frac{\partial g(Q_e)}{\partial Q_e} = \beta * \left(-e^{-Q_e * \beta * \left(2*t_r + \frac{v_c}{a} \right)} * \beta * \left(2*t_r + \frac{v_c}{a} \right) - e^{-Q_e * \beta * \left(3*t_r + \frac{v_c}{a} + \frac{6}{5} \right)} * \beta \right. \\ &\quad * \left(3*t_r + \frac{v_c}{a} * \frac{6}{5} \right) - e^{-Q_e * \beta * \left(4*t_r + \frac{v_c}{a} + \frac{8}{5} \right)} * \beta * \left(4*t_r + \frac{v_c}{a} * \frac{8}{5} \right) \\ &\quad - e^{-Q_e * \beta * \left(5*t_r + \frac{v_c}{a} + \frac{11}{5} \right)} * \beta * \left(5*t_r + \frac{v_c}{a} * \frac{11}{5} \right) - e^{-Q_e * \beta * \left(6*t_r + \frac{v_c}{a} + \frac{15}{5} \right)} * \beta \\ &\quad \left. * \left(6*t_r + \frac{v_c}{a} * \frac{15}{5} \right) \right. \\ &\quad \left. - e^{-Q_e * \beta * \left(7*t_r + 4 * \frac{v_c}{a} \right)} * \beta * \left(7*t_r + 4 * \frac{v_c}{a} \right) \left(1 - e^{-Q_e * \beta * \left(t_r + \frac{v_c}{a} \right)} \right) \right. \\ &\quad \left. \left(1 - e^{-Q_e * \left(t_r + \frac{v_c}{a} \right)} \right)^2 \right) \\ &\quad \left. - e^{-Q_e * \beta * \left(7*t_r + 4 * \frac{v_c}{a} \right)} * e^{-Q_e * \beta * \left(t_r + \frac{v_c}{a} \right)} * \beta * \left(t_r + \frac{v_c}{a} \right) \right) \left/ 0 \right. \\ &\quad \left. \left(1 - e^{-Q_e * \beta * \left(t_r + \frac{v_c}{a} \right)} \right)^2 \right) \end{aligned}$$

B.7. Derivation of $P(S_1 \rightarrow S_2 \rightarrow S_3 \rightarrow \dots \rightarrow S_n \rightarrow S_1)$ in Eq. (19)

$$\begin{aligned} P(S_1 \rightarrow S_2 \rightarrow S_3 \rightarrow \dots \rightarrow S_n \rightarrow S_1) &= P(S_1 \rightarrow S_2) * P(S_2 \rightarrow S_3) * P(S_3 \rightarrow S_4) * \dots * P(S_n \rightarrow S_1) \\ &= e^{-\lambda^O * \left(2*t_r + \frac{v_c^O}{a} \right)} - \lambda^I * \left(2*t_r + \frac{v_c^O + J}{a} \right) * e^{-\lambda^O * \left(t_r + \frac{v_c^O}{a} \right)} - \lambda^I * \left(t_r + \frac{v_c^O}{a} \right) * e^{-\lambda^O * (n-2) * \left(t_r + \frac{v_c^O}{a} \right)} - \lambda^I * (n-2) * \left(t_r + \frac{v_c^O}{a} \right) \\ &\quad * \left(1 - e^{-\lambda^O * \left(t_r + \frac{v_c^O}{a} \right)} - \lambda^I * \left(t_r + \frac{v_c^O}{a} \right) \right) \\ &= e^{-\lambda^O * \left((n+1)*t_r + \frac{v_c^O + \sum_{i=1}^{n-1} v_c^O}{a} \right)} - \lambda^I * \left((n+1)*t_r + \frac{n*v_c^O + J}{a} \right) \\ &= e^{-\lambda^O * \left((n+2)*t_r + \frac{v_c^O + \sum_{i=1}^n v_c^O}{a} \right)} - \lambda^I * \left((n+2)*t_r + \frac{(n+1)*v_c^O + J}{a} \right) \end{aligned}$$

B.8. Derivation of $N_1(T, Q_c, v_c, v_e)$

$$\begin{aligned} N_1^L(T, Q_c^O, Q_c^I, v_c^O, v_c^I, v_e^O) &= T * \min(Q_c^O, Q_c^I) \\ &\quad * \sum_{n=1}^5 * \left(e^{-\lambda^O * \left((n+1)*t_r + \frac{v_c^O + \sum_{i=1}^{n-1} v_c^O}{a} \right)} - \lambda^I * \left((n+1)*t_r + \frac{n*v_c^O + J}{a} \right) \right. \\ &\quad \left. - e^{-\lambda^O * \left((n+2)*t_r + \frac{v_c^O + \sum_{i=1}^n v_c^O}{a} \right)} - \lambda^I * \left((n+2)*t_r + \frac{(n+1)*v_c^O + J}{a} \right) \right) \\ &= T * \min(Q_c^O, Q_c^I) * \left[1 * \left(e^{-\lambda^O * \left((1+1)*t_r + \frac{v_c^O + \sum_{i=1}^{1-1} v_c^O}{a} \right)} - \lambda^I * \left((1+1)*t_r + \frac{1*v_c^O + J}{a} \right) \right. \right. \\ &\quad \left. \left. - e^{-\lambda^O * \left((1+2)*t_r + \frac{v_c^O + \sum_{i=1}^1 v_c^O}{a} \right)} - \lambda^I * \left((1+2)*t_r + \frac{(1+1)*v_c^O + J}{a} \right) \right) \\ &\quad + 2 * \left(e^{-\lambda^O * \left((2+1)*t_r + \frac{v_c^O + \sum_{i=1}^{2-1} v_c^O}{a} \right)} - \lambda^I * \left((2+1)*t_r + \frac{2*v_c^O + J}{a} \right) \right. \\ &\quad \left. - e^{-\lambda^O * \left((2+2)*t_r + \frac{v_c^O + \sum_{i=1}^2 v_c^O}{a} \right)} - \lambda^I * \left((2+2)*t_r + \frac{(2+1)*v_c^O + J}{a} \right) \right) + 3 \\ &\quad * \left(e^{-\lambda^O * \left((3+1)*t_r + \frac{v_c^O + \sum_{i=1}^{3-1} v_c^O}{a} \right)} - \lambda^I * \left((3+1)*t_r + \frac{3*v_c^O + J}{a} \right) \right. \\ &\quad \left. - e^{-\lambda^O * \left((3+2)*t_r + \frac{v_c^O + \sum_{i=1}^3 v_c^O}{a} \right)} - \lambda^I * \left((3+2)*t_r + \frac{(3+1)*v_c^O + J}{a} \right) \right) \end{aligned}$$

$$\begin{aligned}
& +4 * \left(e^{-\lambda^O * \left((4+1)*t_r + \frac{v_c^O + \sum_{i=1}^{4-1} v_{e,i}^O}{a} \right)} - \lambda^I * \left((4+1)*t_r + \frac{4*v_c^O + v_c^I}{a} \right) - e^{-\lambda^O * \left((4+2)*t_r + \frac{v_c^O + \sum_{i=1}^4 v_{e,i}^O}{a} \right)} - \lambda^I * \left((4+2)*t_r + \frac{(4+1)*v_c^O + v_c^I}{a} \right) \right) \\
& +5 * \left(e^{-\lambda^O * \left((5+1)*t_r + \frac{v_c^O + \sum_{i=1}^5 v_{e,i}^O}{a} \right)} - \lambda^I * \left((5+1)*t_r + \frac{5*v_c^O + v_c^I}{a} \right) - e^{-\lambda^O * \left((5+2)*t_r + \frac{v_c^O + \sum_{i=1}^5 v_{e,i}^O}{a} \right)} - \lambda^I * \left((5+2)*t_r + \frac{(5+1)*v_c^O + v_c^I}{a} \right) \right) \Big] \\
& = T * \min(Q_c^O, Q_c^I) * \left[e^{-\lambda^O * \left(2*t_r + \frac{v_c^O}{a} \right)} - \lambda^I * \left(2*t_r + \frac{v_c^O + v_c^I}{a} \right) + e^{-\lambda^O * \left(3*t_r + \frac{6*v_c^O}{a} \right)} - \lambda^I * \left(3*t_r + \frac{2*v_c^O + v_c^I}{a} \right) + e^{-\lambda^O * \left(4*t_r + \frac{8*v_c^O}{a} \right)} - \lambda^I * \left(4*t_r + \frac{3*v_c^O + v_c^I}{a} \right) \right. \\
& \quad \left. + e^{-\lambda^O * \left(5*t_r + \frac{11*v_c^O}{a} \right)} - \lambda^I * \left(5*t_r + \frac{4*v_c^O + v_c^I}{a} \right) + e^{-\lambda^O * \left(6*t_r + \frac{15*v_c^O}{a} \right)} - \lambda^I * \left(6*t_r + \frac{5*v_c^O + v_c^I}{a} \right) - 5e^{-\lambda^O * \left(7*t_r + \frac{19*v_c^O}{a} \right)} - \lambda^I * \left(7*t_r + \frac{6*v_c^O + v_c^I}{a} \right) \right] \\
& + e
\end{aligned}$$

B.9 Derivation of $N_2^L(T, Q_c^O, Q_c^I, v_c^O, v_c^I, v_e^O)$

$$\begin{aligned}
N_2(T, Q_c^O, Q_c^I, v_c^O, v_c^I, v_e^O) & = T * \min(Q_c^O, Q_c^I) \\
& * \sum_{n=6}^{\infty} n * \left[e^{-\lambda^O * \left((n+1)*t_r + \frac{v_c^O + \sum_{i=1}^{n-1} v_{e,i}^O}{a} \right)} - \lambda^I * \left((n+1)*t_r + \frac{n*v_c^O + v_c^I}{a} \right) - e^{-\lambda^O * \left((n+2)*t_r + \frac{v_c^O + \sum_{i=1}^n v_{e,i}^O}{a} \right)} - \lambda^I * \left((n+2)*t_r + \frac{(n+1)*v_c^O + v_c^I}{a} \right) \right) \\
& = T * Q_c * \left[6 * \left(e^{-\lambda^O * \left((6+1)*t_r + \frac{v_c^O + \sum_{i=1}^{6-1} v_{e,i}^O}{a} \right)} - \lambda^I * \left((6+1)*t_r + \frac{6*v_c^O + v_c^I}{a} \right) - e^{-\lambda^O * \left((6+2)*t_r + \frac{v_c^O + \sum_{i=1}^6 v_{e,i}^O}{a} \right)} - \lambda^I * \left((6+2)*t_r + \frac{(6+1)*v_c^O + v_c^I}{a} \right) \right) + 7 \right. \\
& \quad \left. * \left(e^{-\lambda^O * \left((7+1)*t_r + \frac{v_c^O + \sum_{i=1}^{7-1} v_{e,i}^O}{a} \right)} - \lambda^I * \left((7+1)*t_r + \frac{7*v_c^O + v_c^I}{a} \right) - e^{-\lambda^O * \left((7+2)*t_r + \frac{v_c^O + \sum_{i=1}^7 v_{e,i}^O}{a} \right)} - \lambda^I * \left((7+2)*t_r + \frac{(7+1)*v_c^O + v_c^I}{a} \right) \right) + 8 \right. \\
& \quad \left. * \left(e^{-\lambda^O * \left((8+1)*t_r + \frac{v_c^O + \sum_{i=1}^{8-1} v_{e,i}^O}{a} \right)} - \lambda^I * \left((8+1)*t_r + \frac{8*v_c^O + v_c^I}{a} \right) - e^{-\lambda^O * \left((8+2)*t_r + \frac{v_c^O + \sum_{i=1}^8 v_{e,i}^O}{a} \right)} - \lambda^I * \left((8+2)*t_r + \frac{(8+1)*v_c^O + v_c^I}{a} \right) \right) + \dots + N \right. \\
& \quad \left. * \left(e^{-\lambda^O * \left((N+1)*t_r + \frac{v_c^O + \sum_{i=1}^{N-1} v_{e,i}^O}{a} \right)} - \lambda^I * \left((N+1)*t_r + \frac{N*v_c^O + v_c^I}{a} \right) - e^{-\lambda^O * \left((N+2)*t_r + \frac{v_c^O + \sum_{i=1}^N v_{e,i}^O}{a} \right)} - \lambda^I * \left((N+2)*t_r + \frac{(N+1)*v_c^O + v_c^I}{a} \right) \right) \right] \\
& = T * Q_c * \left[6 * e^{-\lambda^O * \left(7*t_r + \frac{4*v_c^O}{a} \right)} - \lambda^I * \left(7*t_r + \frac{6*v_c^O + v_c^I}{a} \right) + e^{-\lambda^O * \left(8*t_r + \frac{5*v_c^O}{a} \right)} - \lambda^I * \left(8*t_r + \frac{7*v_c^O + v_c^I}{a} \right) \right. \\
& \quad \left. - e^{-\lambda^O * \left(7*t_r + \frac{4*v_c^O}{a} \right)} - \lambda^I * \left(7*t_r + \frac{6*v_c^O + v_c^I}{a} \right) + e^{-\lambda^O * \left(8*t_r + \frac{5*v_c^O}{a} \right)} - \lambda^I * \left(8*t_r + \frac{7*v_c^O + v_c^I}{a} \right) * e^{-\lambda^O * \left((N+2)*t_r + \frac{(N-1)*v_c^O}{a} \right)} - \lambda^I * \left((N+2)*t_r + \frac{(N+1)*v_c^O + v_c^I}{a} \right) \right] \\
& - Ne^{-\lambda^O * \left((N+2)*t_r + \frac{(N-1)*v_c^O}{a} \right)} - \lambda^I * \left((N+2)*t_r + \frac{(N+1)*v_c^O + v_c^I}{a} \right) \\
& = T * \min(Q_c^O, Q_c^I) * \left[6 * e^{-\lambda^O * \left(7*t_r + \frac{4*v_c^O}{a} \right)} - \lambda^I * \left(7*t_r + \frac{6*v_c^O + v_c^I}{a} \right) + \lim_{N \rightarrow \infty} \sum_{i=6}^{N-1} e^{-\lambda^O * \left((i+2)*t_r + \frac{(i-1)*v_c^O}{a} \right)} - \lambda^I * \left((i+2)*t_r + \frac{(i+1)*v_c^O + v_c^I}{a} \right) \right. \\
& \quad \left. - \lim_{N \rightarrow \infty} Ne^{-\lambda^O * \left((N+2)*t_r + \frac{(N-1)*v_c^O}{a} \right)} - \lambda^I * \left((N+2)*t_r + \frac{(N+1)*v_c^O + v_c^I}{a} \right) \right]
\end{aligned}$$

B.10 Derivation of $\lim_{N \rightarrow \infty} \sum_{i=5}^{N-1} e^{-\lambda^O * \left((i+2)*t_r + \frac{(i-1)*v_c^O}{a} \right)} - \lambda^I * \left((i+2)*t_r + \frac{(i+1)*v_c^O + v_c^I}{a} \right)$

$$\begin{aligned}
& \lim_{N \rightarrow \infty} \sum_{i=5}^{N-1} e^{-\lambda^O * \left((i+2)*t_r + \frac{(i-1)*v_c^O}{a} \right)} - \lambda^I * \left((i+2)*t_r + \frac{(i+1)*v_c^O + v_c^I}{a} \right) \\
& = \lim_{N \rightarrow \infty} \frac{e^{-\lambda^O * \left(7*t_r + \frac{4*v_c^O}{a} \right)} - \lambda^I * \left(7*t_r + \frac{6*v_c^O + v_c^I}{a} \right) * \left(1 - e^{N * \left(-\lambda^O * \left(t_r + \frac{v_c^O}{a} \right) - \lambda^I * \left(t_r + \frac{v_c^O}{a} \right) \right)} \right)}{1 - e^{-\lambda^O * \left(t_r + \frac{v_c^O}{a} \right)} - \lambda^I * \left(t_r + \frac{v_c^O}{a} \right)} \\
& = \frac{e^{-\lambda^O * \left(7*t_r + \frac{4*v_c^O}{a} \right)} - \lambda^I * \left(7*t_r + \frac{6*v_c^O + v_c^I}{a} \right) * \lim_{N \rightarrow \infty} \left(1 - e^{N * \left(-\lambda^O * \left(t_r + \frac{v_c^O}{a} \right) - \lambda^I * \left(t_r + \frac{v_c^O}{a} \right) \right)} \right)}{1 - e^{-\lambda^O * \left(t_r + \frac{v_c^O}{a} \right)} - \lambda^I * \left(t_r + \frac{v_c^O}{a} \right)} \\
& = \frac{e^{-\lambda^O * \left(7*t_r + \frac{4*v_c^O}{a} \right)} - \lambda^I * \left(7*t_r + \frac{6*v_c^O + v_c^I}{a} \right) * (1 - 0)}{1 - e^{-\lambda^O * \left(t_r + \frac{v_c^O}{a} \right)} - \lambda^I * \left(t_r + \frac{v_c^O}{a} \right)} = \frac{e^{-\lambda^O * \left(7*t_r + \frac{4*v_c^O}{a} \right)} - \lambda^I * \left(7*t_r + \frac{6*v_c^O + v_c^I}{a} \right)}{1 - e^{-\lambda^O * \left(t_r + \frac{v_c^O}{a} \right)} - \lambda^I * \left(t_r + \frac{v_c^O}{a} \right)} \\
& \underline{\text{B.11 Derivation of } \lim_{N \rightarrow \infty} N e^{-\lambda^O * \left((N+2)*t_r + \frac{(N-1)*v_c^O}{a} \right)} - \lambda^I * \left((N+2)*t_r + \frac{(N+1)*v_c^O + v_c^I}{a} \right) }
\end{aligned}$$

$$\begin{aligned}
& \lim_{N \rightarrow \infty} N e^{-\lambda^O * \left((N+2)*t_r + \frac{(N-1)*v_c^O}{a} \right)} - \lambda^I * \left((N+2)*t_r + \frac{(N+1)*v_c^O + v_c^I}{a} \right) = \lim_{N \rightarrow \infty} \frac{N}{e^{\lambda^O * \left((N+2)*t_r + \frac{(N-1)*v_c^O}{a} \right) + \lambda^I * \left((N+2)*t_r + \frac{(N+1)*v_c^O + v_c^I}{a} \right)}} \\
& = \lim_{N \rightarrow \infty} \frac{1}{\left(\lambda^O * \left(t_r + \frac{v_c^O}{a} \right) + \lambda^I * \left(t_r + \frac{v_c^O}{a} \right) \right) * e^{\lambda^O * \left((N+2)*t_r + \frac{(N-1)*v_c^O}{a} \right) + \lambda^I * \left((N+2)*t_r + \frac{(N+1)*v_c^O + v_c^I}{a} \right)}} = 0
\end{aligned}$$

References

- Akcelik, R., 1994. Gap-acceptance modelling by traffic signal analogy. *Traffic Engineering & Control* 35 (9), 498–501.
- Akcelik, R., 2007. A review of gap-acceptance capacity models. The 29th Conference of Australian Institutes of Transport Research (CAITR 2007). University of South Australia, Adelaide, Australia.
- Akcelik, R., 2011. An assessment of the Highway Capacity Manual 2010 roundabout capacity model. In: TRB International Roundabout Conference. Carmel, Indiana, USA.
- Akcelik, R., E. Chung and M. Besley (1998). Roundabouts: Capacity and performance analysis.
- Breuer, A., J.-A. Termöhlen, S. Homoceanu and T. Fingscheidt (2020). "openDD: A large-scale roundabout drone dataset." arXiv preprint arXiv:2007.08463.
- Brilon, W., Stuwe, B., 1993. Capacity and design of traffic circles in Germany. *Transp. Res. Rec.* 61–61.
- Brilon, W., Wu, N., Bondzio, L., 1997. Unsignalized intersections in Germany. A state of the art 1997. In: Proceedings of the third international symposium on intersections without traffic signals.
- Bunker, J., Troutbeck, R., 2003. Prediction of minor stream delays at a limited priority freeway merge. *Transp. Res. Part B Methodol.* 37 (8), 719–735.
- Chen, R., Hourdos, J., 2018. Evaluation of the Roundabout Capacity Model in HCM6 Edition and HCM 2010 on a Multilane Roundabout. *Transp. Res.* 2672 (15), 23–34.
- Fambro, D.B., Fitzpatrick, K., Koppa, R.J., 1997. Determination of stopping sight distances. *Transportation Research Board*.
- Fisk, C.S., 1991. Traffic performance analysis at roundabouts. *Transp. Res. Part B Methodol.* 25 (2), 89–102.
- Fitzpatrick, C.D., Abrams, D.S., Tang, Y., Knodler Jr, M.A., 2013. Spatial and temporal analysis of driver gap acceptance behavior at modern roundabouts. *Transp. Res.* Rec. 2388 (1), 14–20.
- Gazzari, A., Martello, M., Pratelli, A., Souleyrette, R., 2013. Gap acceptance parameters for HCM 2010 roundabout capacity model applications in Italy. *Intersections Control and Safety. Transportation Systems & Traffic Engineering*. WitPress, Southampton. Boston, pp. 1–16.
- Guo, R., Liu, L., Wang, W., 2019. Review of roundabout capacity based on gap acceptance. *J. Adv. Transp.* 2019.
- Hagring, O., 1998. A further generalization of Tanner's formula. *Transp. Res. Part B Methodol.* 32, 423–429.
- Hao, H., Ma, W., 2017. Revisiting distribution model of departure headways at signalised intersections. *Transportmetrica B: transport dynamics* 5 (1), 1–14.
- Henry, R. D. and W. Sabra. (2005). "Signal timing on a shoestring".
- Jin, X., Zhang, Y., Wang, F., Li, L., Yao, D., Su, Y., Wei, Z., 2009. Departure headways at signalized intersections: A log-normal distribution model approach. *Transp. Res. Part C Emerging Technol.* 17 (3), 318–327.
- Káčovský, J., Kocourek, J., Padelek, T., 2019. Examination of Logical Trends in Traffic Conflicts and Traffic Accidents in the Context of Road Safety at Roundabouts. In: 2019 Smart City Symposium Prague (SCSP). IEEE.
- Karlaftis, M.G., Vlahogianni, E.I., 2011. Statistical methods versus neural networks in transportation research: Differences, similarities and some insights. *Transp. Res. Part C Emerging Technol.* 19 (3), 387–399.
- Kimber, R. (1980). "The traffic capacity of roundabouts".
- Kociánová, A., 2021. Capacity Model for Single-Lane Minor Entry at Turbo-Roundabouts. *Civ. Environ. Eng.* 17 (1), 318–326.
- Křivda, V. (2005). "Calculation of capacity reserves of small roundabouts arms using capacity calculations of direct intersections & T-junctions".
- Křivda, V., Petru, J., 2017. PROPOSAL OF CAPACITY CALCULATION OF ROUNDABOUT DEPARTURE WITH CYCLE TRAFFIC IN CONDITIONS OF THE CZECH REPUBLIC. International Multidisciplinary Scientific GeoConference: SGEM 17, 721–728.

- Krvida, V., Petru, J., 2018. COMPARISON OF SELECTED CAPACITY CALCULATIONS FOR ROUNDABOUTS. Sofia, Surveying Geology & Mining Ecology Management (SGEM) 18, 519–526.
- Larson, R. C. and A. R. Odoni (1981). Urban operations research.
- Mathew, S., Dhamaniya, A., Arkatkar, S., Joshi, G., 2017. Roundabout capacity in heterogeneous traffic condition: Modification of HCM equation and calibration. *Transp. Res. Procedia* 27, 985–992.
- Özuyal, M., Çalışkanelli, S., Tanyel, S., Baran, T., 2009. Capacity prediction for traffic circles: applicability of ANN. In: Proc. Inst. Civ. Eng. Trans. Thomas Telford Ltd.
- Patnaik, A. K., R. Patra and P. K. Bhuyan (2020). "Comparison of Artificial Intelligence Based Roundabout Entry Capacity Models." *International Journal of Intelligent Transportation Systems Research* 18(2): 288-296.
- Pilko, H., Mandžuka, S., Barić, D., 2017. Urban single-lane roundabouts: A new analytical approach using multi-criteria and simultaneous multi-objective optimization of geometry design, efficiency and safety. *Transp. Res. Part C Emerging Technol.* 80, 257–271.
- Pollatschek, M.A., Polus, A., Livneh, M., 2002. A decision model for gap acceptance and capacity at intersections. *Transp. Res. Part B Methodol.* 36 (7), 649–663.
- Polus, A., Shmueli, S., 1997. Analysis and Evaluation of the Capacity of Roundabouts. *Transp. Res. Rec.* 1572 (1), 99–104.
- Pompigna, A., Guerrieri, M., Mauro, R., 2020. New Extensions and Applications of the Modified Chumanov Model for Calculating Entry Capacity of Single-Lane Roundabouts. *Sustainability* 12 (15), 6122.
- Qu, X., Ren, L., Wang, S., Oh, E., 2014. Estimation of entry capacity for single-lane modern roundabouts: case study in Queensland, Australia. *J. Transp. Eng.* 140 (7), 05014002.
- Ren, L., Qu, X., Guan, H., Easa, S., Oh, E., 2016. Evaluation of Roundabout Capacity Models: An Empirical Case Study. *J. Transp. Eng.* 142 (12), 04016066.
- Robinson, B. W., L. Rodegerdts, W. Scarborough, W. Kittelson, R. Troutbeck, W. Brilon, L. Bondizio, K. Courage, M. Kyte and J. Mason. (2010). "Roundabouts: An informational guide".
- Rodegerdts, L., 2007. NCHRP Report 572. Roundabouts in the United States.
- Rodegerdts, L., Blogg, M., Wemple, E., Myers, E., Kyte, M., Dixon, M., List, G., Flannery, A., Troutbeck, R., Brilon, W., 2007. Appendixes to NCHRP Report 572: Roundabouts in the United States. NCHRP Web-Only Document, p. 94.
- Simon, M.J., 1991. Roundabouts in Switzerland. *Intersections without traffic signals II*. Springer, pp. 41–52.
- Stuwe, B., 1991. Capacity and safety of roundabouts—German results. *Intersections without Traffic Signals II*. Springer, pp. 1–12.
- Tanner, J.C., 1962. A Theoretical Analysis of Delays at an Uncontrolled Intersection. *Biometrika* 49 (1/2), 163–170.
- Tollazzi, T., Srami, M., Lerher, T., 2008. Roundabout arm capacity determined by microsimulation and discrete functions technique. *Promet-Traffic&Transportation* 20 (5), 291–300.
- TRB (2010). Highway Capacity Manual.
- TRB, 2016. Highway Capacity Manual 2016. Transportation Research Board, Washington D.C.
- Troutbeck, R., 1989. Evaluating the Performance of a Roundabout. Australian Road Research Board, Vermont South.
- Troutbeck, R., 2014. Estimating the mean critical gap. *Transp. Res. Rec.* 2461 (1), 76–84.
- Valdez, M., Cheu, R.L., Duran, C., 2011. Operations of modern roundabout with unbalanced approach volumes. *Transp. Res. Rec.* 2265 (1), 234–243.
- Wei, T., Grenard, J.L., 2012. Calibration and validation of highway capacity manual 2010 capacity model for single-lane roundabouts. *Transp. Res. Rec.* 2286 (1), 105–110.
- Wong, S.C., 1996. On the reserve capacities of priority junctions and roundabouts. *Transp. Res. Part B Methodol.* 30 (6), 441–453.
- Wu, N., 2001. A universal procedure for capacity determination at unsignalized (priority-controlled) intersections. *Transp. Res. Part B Methodol.* 35 (6), 593–623.
- Xu, F., Tian, Z.Z., 2008. Driver behavior and gap-acceptance characteristics at roundabouts in California. *Transp. Res. Rec.* 2071 (1), 117–124.
- Yap, Y.H., Gibson, H.M., Waterson, B.J., 2013. An international review of roundabout capacity modelling. *Transport Rev.* 33 (5), 593–616.
- Yap, Y.H., Gibson, H.M., Waterson, B.J., 2015. Models of roundabout lane capacity. *J. Transp. Eng.* 141 (7), 04015007.